

System For Fabricating Thin Film Magnetic Microstructures

by

Todd Charles Monson, B.S.

Thesis

Presented to the Faculty of the Graduate School of

The University of Texas at Austin

in Partial Fulfillment

of the Requirements

for the Degree of

Master of Arts

The University of Texas at Austin

December 2001

DISTRIBUTION STATEMENT A
Approved for Public Release
Distribution Unlimited

System For Fabricating Thin Film Magnetic Microstructures

**Approved by
Supervising Committee:**

Dedication

To my grandmother, Mary Monson, who was my best childhood friend, and to all
those affected by the tragedy of September 11th.

Acknowledgements

Just as with any major project started in the world today, if I had not had a tremendous deal of help along the way, I would not have been able to complete this thesis.

First and foremost, I would like to thank Dr. James Erskine who was very supportive of me earning a Master's Degree, even before I was accepted into UT Austin. His technical expertise and support were helpful every step along the way. In addition, he was very understanding of my obligations outside the lab including my wife and classes.

I would also like to thank Dr. Hector Mireles who was always very willing to share his surface physics expertise and knowledge of the "Erskine lab". In just a few minute conversation with Dr. Mireles, I could walk away with so much valuable information. Plus, he was a very interesting person to work with and made life in the lab so much more enjoyable. Ben Bowes, who worked on his PHY 380N research project in Dr. Erskine's lab was of great assistance this past summer. And it seems that no one can get through graduate school in the UT Austin Physics Department without the assistance of department technician Jack Clifford, who helped tremendously with the early machining tasks of this project.

Of course, I cannot forget the help of my wife, Judy, without whom I could have never made it through all of the wedding plans while studying for my classes and trying to squeeze in whatever research I could along the way. If it wasn't for her it would have been so easy to lose touch with the outside world and forget about what is really important in life.

Finally, I would like to acknowledge the U.S. Air Force and the U.S. Air Force Academy who made my dream of pursuing a Master's degree a reality. If it was not for their faith in me and my abilities I would not be here today.

December 2001

Table of Contents

List of Tables.....	vii
List of Figures	viii
Chapter 1: Introduction	1
Chapter 2: Background.....	4
Chapter 3: System Upgrades	12
MBE Cell.....	12
Sample Holder.....	15
MBE Cell and Substrate Power Supplies.....	17
Bake-Out Electronics	25
Chapter 4: Software Development	30
MBE Instrumentation Software	30
Auger Electron Spectroscopy Software	39
Chapter 5: Preparation For Thin Film Growth.....	43
Achieving UHV.....	43
High Temperature Flash.....	46
Auger Electron Spectroscopy	47
Chapter 6: Evaporations.....	50
Chapter 7: Experimental Calibration.....	55
Chapter 8: Conclusion.....	63
References	65
Vita	67

List of Tables

Table 1: Pin Functions of XTC RS 232 Connector. ¹⁶	32
Table 2: Auger Control Settings That Worked Well For the CMA System	48

List of Figures

Figure 1: Schematic of Domain Wall Pattern in a Permalloy Film Structure. ⁵	3
Figure 2: CMA Thin Film Growth and Analysis Chamber.	5
Figure 3: Figure 3: Side View of the MBE Cell. This view shows the location of the source wire and filament as well as the position and shape of the collector. The sample manipulator is visible through a viewport in the background and the side of the tungsten substrate can barely be discerned.	7
Figure 4: XTC Crystal Monitor. The quartz crystal is to the far left in the photograph. To the far right, are the cooling water feedthrus and a BNC connector.	8
Figure 5: Diagram of a Cylindrical Mirror Analyzer (In Red). The red curves show the path of the Auger electrons, whose energy are proportional to $-V$. The sample, electron gun, and electron multiplier are also shown in this diagram. ¹⁰	10
Figure 6: Diagram of MBE Cell Along With Its Water Cooled Shroud and the Tungsten Substrate.	14
Figure 7: The tungsten filament and iron source can clearly be seen in this photograph of the MBE cell with the collector removed. Both copper wires running parallel to the source and supplying current to the filament have been completely covered with evaporated metal.	15

Figure 8: Filament shape and positioning behind the tungsten substrate that allowed the sample to be flashed consistently. ⁴	17
Figure 9: Front Panel of the Evaporator Power Supply. The sample power supply's front panel is almost identical except that it does not have the extra switch in the middle of the panel to toggle the emission current meter between two different settings.	18
Figure 10: Block Diagram of Evaporator Power Supply. The sample power supply is identical.	19
Figure 11: Substrate Power Supply HV/Emission Meter Circuit.	23
Figure 12: Evaporator Power Supply HV/Emission Meter Circuit. The circuit which measures the emission current has the added feature of two settings: 50mA max. deflection and 500 mA max. deflection.	24
Figure 13: Upgraded Bake-Out Electronics. In the actual circuit, there would be an additional 220 VAC wall plug connected to a second master relay. One 220 VAC plug/relay combination would be connected to three solid state relays and power three heating elements, while the additional plug/relay combination would be connected to the remaining two solid state relays.	28
Figure 14: Front Panel of Upgraded Bake-Out Electronics.	29
Figure 15: Female 9-Pin RS 232 Connector Used On XTC.	32

Figure 16: Initialization Sequence (1 of 4) of XTC VI. The rest of this sequence only contained empty space and was omitted from the figure.	33
Figure 17: Write Data Sequence (2 of 4) of XTC VI. The rest of this sequence only contained empty space and was omitted from the figure.	34
Figure 18: Wait Sequence (3 of 4) of XTC VI. The rest of this sequence only contained empty space and was omitted from the figure.	35
Figure 19: Read Data Sequence (4 of 4) of XTC VI.....	36
Figure 20: User Interface of MBE VI.	37
Figure 21: 'Circuit' Diagram of MBE VI.	38
Figure 22: User Interface of Auger Plotter VI with Auger Spectrum Displayed.....	41
Figure 23: 'Circuit' Diagram of Auger Plotter VI.	42
Figure 24: Permalloy Wire Heated Too Aggressively. When too much emission current was used to heat this wire, the portion of the tip that was melted became too large for its surface tension to hold it in place. The liquid permalloy then fell beneath the wire, leading to very poor evaporation efficiencies.	52
Figure 25: Crystal Monitor Thickness vs. Integrated Ion Flux. The data were taken during a series of Fe evaporations. Both methods of using the crystal monitor data are displayed here.	57

Figure 26: Fe(703)/W(179) Auger signal ratio vs. deposition time. The temperature refers to the substrate temperature during the evaporation. ¹⁷	59
Figure 27: Plot of Fe/W Auger Signal Ratios vs. Integrated Ion Flux Obtained During an Fe Evaporation.....	61
Figure 28: Plot of Permalloy/W Auger Signal Ratios vs. Integrated Ion Flux Obtained During a Permalloy Evaporation.	62

Chapter 1: Introduction

The field of surface physics makes up an important part of condensed matter physics. Surface physics is the study of the physical properties of materials which are influenced by the interface between the material and a vacuum. Phenomena attributed to surface physics are present today in everything from environmental science to electronic devices. However, only since the 1970's have the technology and instruments necessary to study these phenomena been available.

Much of the field of surface physics revolves around the study of metallic thin films. There are many real world applications that utilize thin film technology. Magnetic random-access memories (MRAM) are seen as a possible replacement for the current dynamic random-access memories (DRAM) based on semiconductor technology that are used today. Thin magnetic films would be used in this new non-volatile (retains information when the power is switched off) computer memory.¹

Many sensors and other devices are constructed out of layered magnetic structures. For example, sensors based on phenomena such as giant magnetoresistance (GMR) and tunneling magnetoresistance (TMR) sandwich a nonmagnetic metallic layer (GMR) or an insulating layer (TMR) between magnetic layers.¹ GMR sensors are used as read heads for computer hard drives, which incidentally are also made out of thin films. Through improvements in thin film technology, hard disk density has doubled approximately every five years

and values greater than 30 Gbytes/in² have been achieved. With new advances, hard drive companies are promising 100 Gbytes/in² in the near future. In addition to the examples discussed above, many other devices exploit the properties of thin films. It is important not to neglect the future development of spin electronics, or spintronics, and other technologies based on magnetic properties and thin films.

In addition to their usefulness in commercial devices, thin films are important tools for furthering our understanding of magnetism. Magnetic thin films can be used to research certain kinds of non-linear behavior. They are also ideal for studying the transition between 2-D and 3-D or bulk magnetic behavior. For example, materials that are bulk nonmagnetic can become magnetic in the 2-D regime while some ferromagnetic materials will lose their magnetic behavior in a thin film only a few monolayers (MLs) thick.^{2,3}

In thin films, the symmetry perpendicular to the surface of the film is removed, leading to a magnetic anisotropy or a preferred direction of the magnetic moment.⁴ One area of interest is how magnetic reversal occurs in thin films in the presence of an external magnetic field. Both nucleation and domain wall (the separation between two regions of preferred spin orientation) propagation are ways of magnetic reversal occurring. The conditions under which each situation occurs, and the manner in which they occur, can be studied by using the magneto-optical Kerr effect. The Kerr effect measures the polarization rotation of light reflected off of a magnetic surface. In addition, the same experiments can be performed on thin film nanostructures, which adds yet another level of complexity to the study of magnetic domain behavior.

The choice of materials used to study magnetic behavior can also affect the observations. A common material used is Iron (Fe).⁴ Soft-magnetic materials, or materials that can be made to reverse their magnetization direction with relative ease, have always been desired. Permalloy ($\text{Ni}_{0.8}\text{Fe}_{0.2}$) turned out to be a very good soft-magnetic material. In addition to being soft-magnetic in its bulk form, permalloy is able to preserve its soft-magnetic behavior even when in thin film form.¹ A schematic of the domain wall patterns in a permalloy structure can be seen in Figure 1.

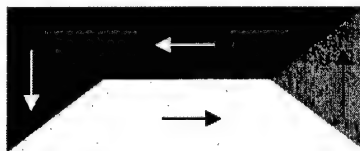


Figure 1: Schematic of Domain Wall Pattern in a Permalloy Film Structure.⁵

The goal of this project is to recondition and improve an Ultra High Vacuum (UHV) system in order to use it to develop high quality and well characterized magnetic films. This involves upgrading and repairing instrumentation used in both thin film growth and characterization. Most importantly, we will develop and calibrate a sensitive flux sensor to monitor film growth.

Chapter 2: Background

With the reasons clear for studying thin films, we must have a method for preparing them for research. In order to study many of these effects, the thin films must be grown in-house in UHV, which means a pressure of 1×10^{-10} Torr or less. Pressures near the UHV regime are necessary in order to reduce the rate at which gas and other contaminants adsorb onto the surface. Contaminants could change a film's surface characteristics and the results of any experiment being performed. Additionally, higher pressures make less than ideal conditions for thin film growth.

In order to grow thin metallic films, we planned to use a vacuum chamber system that has been in operation since approximately 1980. In addition to a Molecular Beam Epitaxy (MBE) cell for film growth, this chamber also incorporates a Low Energy Electron Diffraction (LEED) system and an Auger Electron Spectroscopy (AES) system based on a Cylindrical Mirror Analyzer (CMA). Both LEED and AES are used for surface analysis. In our lab, this particular vacuum chamber is referred to as the CMA system. A picture of the CMA system and some of its instrumentation can be seen in Figure 2.

We needed a method of growing films of a known thickness using this chamber. A calibration for thin film growth in this particular system needed to be developed. Since films only a few atomic layers thick were desired, it was not possible for these films to stand on their own. Some sort of substrate, often tungsten (W) in a 100 crystal orientation is used. Tungsten is both non-magnetic

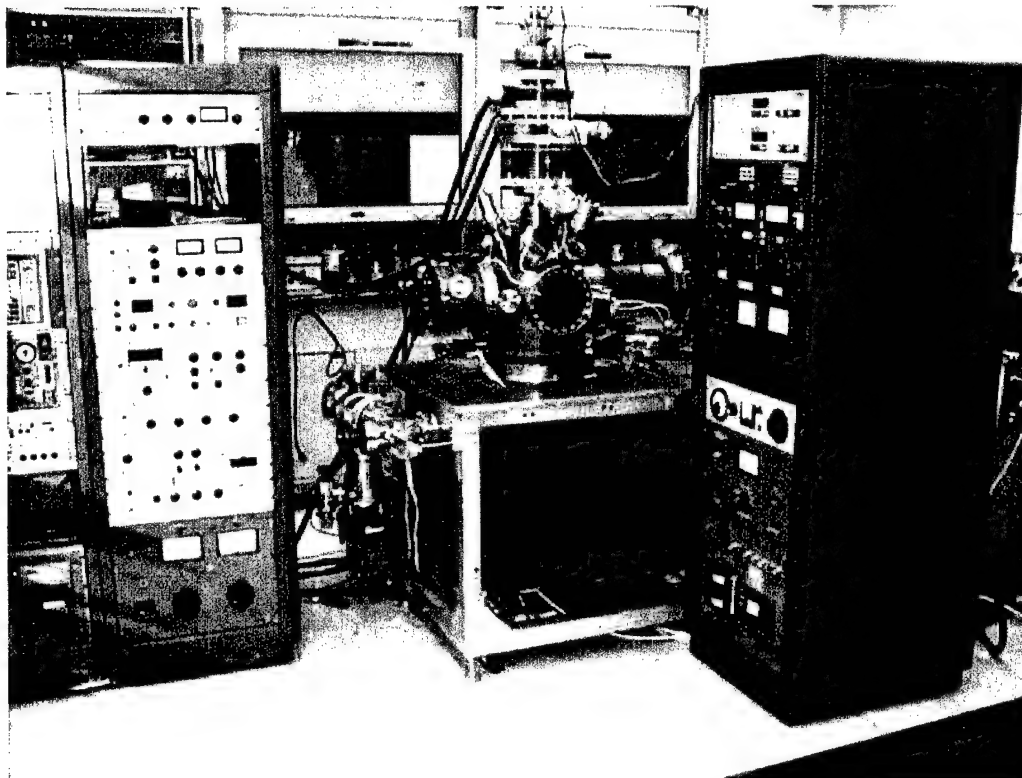


Figure 2: CMA Thin Film Growth and Analysis Chamber.

and has an extremely high melting point (3385 °C). This high melting point enables the crystal to be flashed (raised to an extremely high temperature through e-beam heating) in order to remove any surface contaminants or layers of metal deposited earlier.⁴ Tungsten is extremely useful when developing calibration curves for a system since many evaporations must be performed. Once a calibration run is completed the W crystal can be flashed, removing any deposited layers, and another calibration run can start from a “clean slate”.

During thin film growth relatively slow rates of deposition are desired in order to produce even epitaxial growth and prevent islanding or clustering of the

deposited material. Typically, rates of 0.1 – 1 MLs per minute are desired. A ML represents one atomic layer of a particular material. We used a home made pendant-drop type Electron Beam (EB) MBE cell for thin film growth. In this case, a piece of high purity metal wire is connected to a high voltage (HV) supply. A grounded W filament is wrapped in a tight corkscrew shape in close proximity to the Fe wire. Normally, the metal wire is held at a bias voltage close to +1 kV while several amps of current are passed through the W filament, causing the metal wire to be e-beam heated and in turn evaporated. The entire MBE cell is water cooled in order to reduce outgassing. A photograph of the MBE cell with the sample holder visible through a vacuum chamber viewport in background is shown in Figure 3.

The choice of an EB evaporator over a Knudsen Cell (KC) evaporator does limit us to materials possessing high melting points. However, it does reduce the outgassing of the source. Additionally, an EB evaporator requires a smaller current supply than a KC and needs less space, which is useful in most experimental vacuum chambers.⁶

There are two methods of measuring both the deposition rate and thickness during an evaporation. Within the MBE cell we placed a commercial thickness monitor.⁷ The XTC thickness monitor measures both deposition rate and film thickness by monitoring the resonant frequency of a quartz crystal located within the MBE cell. A picture of the XTC crystal is shown in Figure 4.

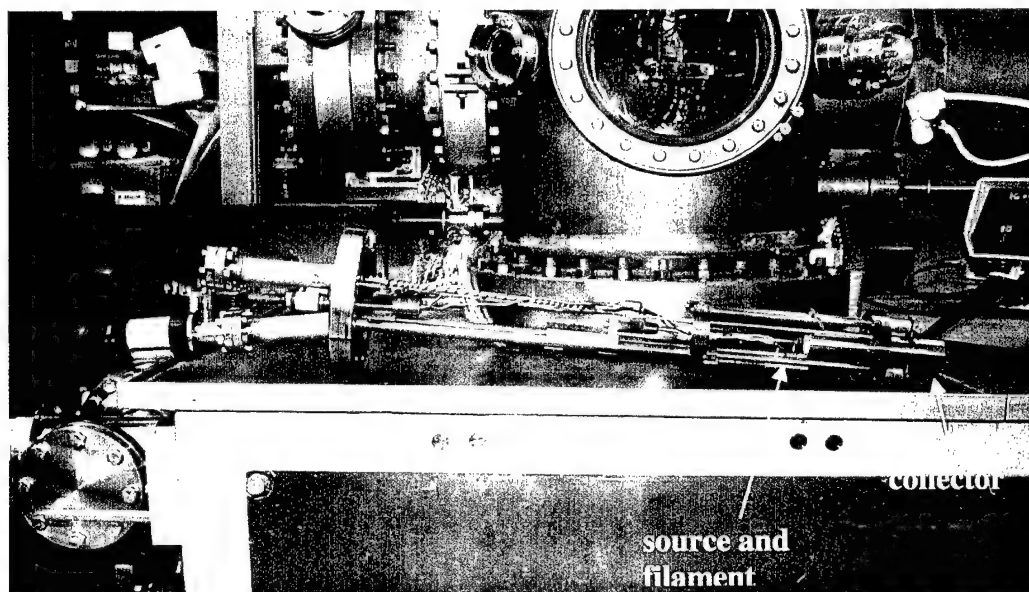


Figure 3: Side View of the MBE Cell. This view shows the location of the source wire and filament as well as the position and shape of the collector. The sample manipulator is visible through a viewport in the background and the side of the tungsten substrate can barely be discerned.

Additionally, the deposition rate can be tracked by measuring the ion current. During the evaporation process, positively charged ions are produced (a fraction of the metallic wire is ionized). By placing a negative bias of approximately -50 V on a metal tube located within the MBE cell called the collector, an ion current can be measured using an electrometer or picoammeter. The ion current is proportional to the deposition rate to a very close approximation.⁸ Additionally, by integrating the ion current over the course of an evaporation, the total deposited thickness can be determined, provided the system is suitably calibrated. The ion current measurement can eliminate many of the shortcomings of the crystal monitor. In the case of the CMA thin film growth chamber, the crystal thickness monitor is close to the filament in the MBE cell.

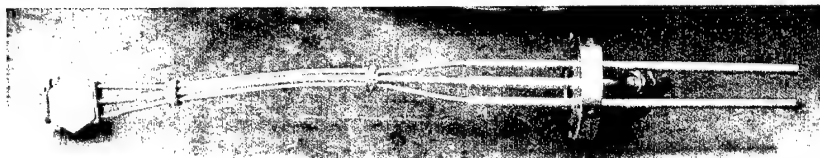


Figure 4: XTC Crystal Monitor. The quartz crystal is to the far left in the photograph. To the far right, are the cooling water feedthrus and a BNC connector.

The filament radiates a considerable amount of heat, which can affect the readings of the thickness monitor (thermal drift), despite the fact that the crystal is water cooled during an evaporation. Additionally, an ion current monitoring device can be a much more sensitive flux monitor than a crystal monitor.

The various analyzing instruments available to characterize both the substrate and thin film were mentioned in this chapter's second paragraph. The only characterization technique used during this project was AES. A sensitivity of 1% of a monolayer can be achieved with AES, which is extremely useful when calibrating a thin film growth system.⁹

The vacuum chamber used for this project is equipped with a commercial CMA manufactured by Physical Electronics. Other electron energy analyzers do exist, however most modern instruments are based on CMA technology since it has a higher signal-to-noise ratio due to its higher transmission efficiency.¹⁰

In order to perform AES an electron gun within the CMA bombards the surface of the sample with an electron beam of several kV in energy, which ejects valence or core level electrons via an Auger process. In the Auger process, the electron beam first ejects an inner shell atomic electron of binding energy E_i . The vacancy created is then filled by a higher lying core or valence electron of binding

energy E_2 , which occurs along with a simultaneous release of energy. Finally, a third electron of binding energy E_3 , the Auger electron, escapes carrying the excess energy previously released. Thus, the Auger electron carries kinetic energy: $E_{K.E.} = E_1 - E_2 - E_3$.⁴ The kinetic energy of these Auger electrons is a property of the element itself and is tabulated in the AES handbook.¹¹ AES is a surface specific method of characterization since electrons emerging from deeper than 1 – 5 nm will suffer strong attenuation resulting from the short electron escape depth.¹²

The Auger electrons move out in all directions. Some of these electrons pass through the CMA's grid covered aperture where they are steered by a variable negative potential on the CMA's outer cylinder. These electrons then pass through an aperture in the inner cylinder followed by an aperture on the CMA's central axis. Those electrons transmitted through all three apertures have an energy that is proportional to the negative voltage of the outer cylinder.¹⁰ The analyzer electronics scan across a range of kinetic energies in order to measure a spectrum. A diagram of a CMA showing the path of measured Auger electrons as well as additional AES components is shown in Figure 5.

Once the electrons pass through the final aperture, an electron multiplier acts as a high gain amplifier. Then, analog circuitry and a lockin amplifier are used to provide a differentiated spectra ($dN(E)/dE$). The values of $dN(E)/dE$ vs. energy (eV) are plotted to make the Auger electrons more apparent against the background of electrons bombarding the analyzer that have undergone many scattering processes. Typically, the output from the AES electronics is sent to a

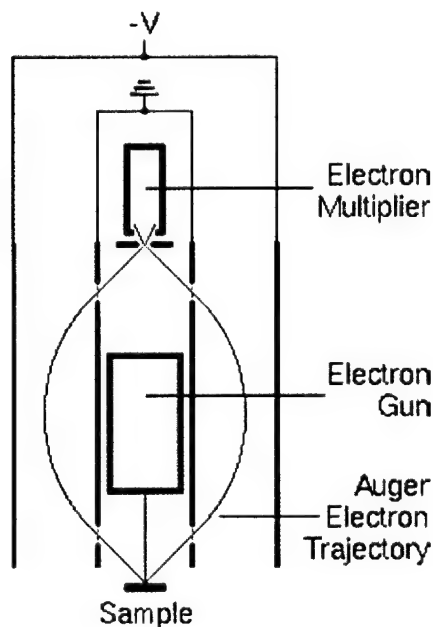


Figure 5: Diagram of a Cylindrical Mirror Analyzer (In Red). The red curves show the path of the Auger electrons, whose energy are proportional to $-V$. The sample, electron gun, and electron multiplier are also shown in this diagram.¹⁰

pen and paper plotter. The peaks can be identified and measured with a ruler in order to determine not only the elements present but their relative concentrations.

Our project focused first on preparing the vacuum system to perform evaporations and then on improving film growth capabilities. This involved correcting deficiencies and modifying the current system. Various parts of the system were upgraded including the MBE cell itself, the sample manipulator, evaporation and flashing power supplies, as well as the bake-out control electronics. In addition, Labview software was developed to monitor the film growth process and record AES spectra. Once the system was ready to perform evaporations, we had to develop our growth techniques and determine what conditions produced the best film growth. Finally, a growth calibration needed to

be produced to ensure that the system could consistently develop metallic microstructures suitable for further research.

Chapter 3: System Upgrades

MBE CELL

A number of tasks needed to be accomplished in order to prepare the MBE cell. Since the metal wire must be held near +1 kV and several amps of current must be passed through the W filament in close proximity to the wire, a number of ceramic standoffs are used in the design of the MBE cell. Through experience, our lab has learned that when these ceramic standoffs are sandwiched between two pieces of metal a “virtual leak” can form when the system is brought down to vacuum. In a “virtual leak”, gas trapped where the standoff is in contact with the adjoining metal will slowly escape and the pressure of the system will not reach the desired levels.

In order to prevent “virtual leaks”, a small slit was cut on both ends of all ceramic standoffs in the MBE cell. A circular diamond saw is the best tool for making these small incisions into the ceramic standoff. Once the standoff was positioned on the diamond saw, the saw’s counterweight was adjusted to apply a light pressure between the standoff and the diamond saw’s cutting blade. This allowed a slit to be cut in the standoff in approximately 15-20 minutes.

Additionally, the wires supplying both the High Voltage (HV) and current to the MBE cell were run through ceramic insulators. These ceramic insulators had to be cut to the appropriate length. Once again, the circular diamond saw was an excellent cutting tool.

Next, we chose to use a small piece of stainless steel as a mirror to observe the position of the metal wire tip in relation to center of the W filament coils. For ideal evaporation conditions, the metal wire tip should be centered within the W filament coils. However, as the metal source is evaporated, the tip recedes away from the filament. Our MBE cell was designed so that the wire can be advanced or retracted with a linear motion feethru in the vacuum chamber. A mirror inside the chamber could allow the position of the wire tip to be determined and adjusted if necessary.

The stainless steel piece was polished in our lab until it reached mirror smoothness. When the MBE cell was placed inside the vacuum chamber, however, there was insufficient lighting to determine the tip's position. Both the filament and the tip emit a great deal of light during an evaporation but then the light is too intense to look at.

The entire MBE cell fits into a water cooled shroud and some parts of the MBE cell had to be ground down in order to fit into this shroud. The XTC crystal monitor head had to be bent in order to be positioned inside of the shroud so that its crystal would receive the flux from the evaporating tip (the metal shafts which support the crystal itself can be bent to a some extent). Just like the MBE cell, the XTC crystal can be water cooled during an evaporation. The XTC crystal chosen was a bakeable crystal which allowed the system to be baked without having to worry about damaging the thickness monitor. At the end of the water cooled shroud is a mechanical shutter that can be used to shut off the MBE cell from the rest of the vacuum chamber. Figure 6 is a schematic of the MBE cell along with

its water cooled shroud. The relative placement of the crystal monitor and the substrate can also be seen in Figure 6.

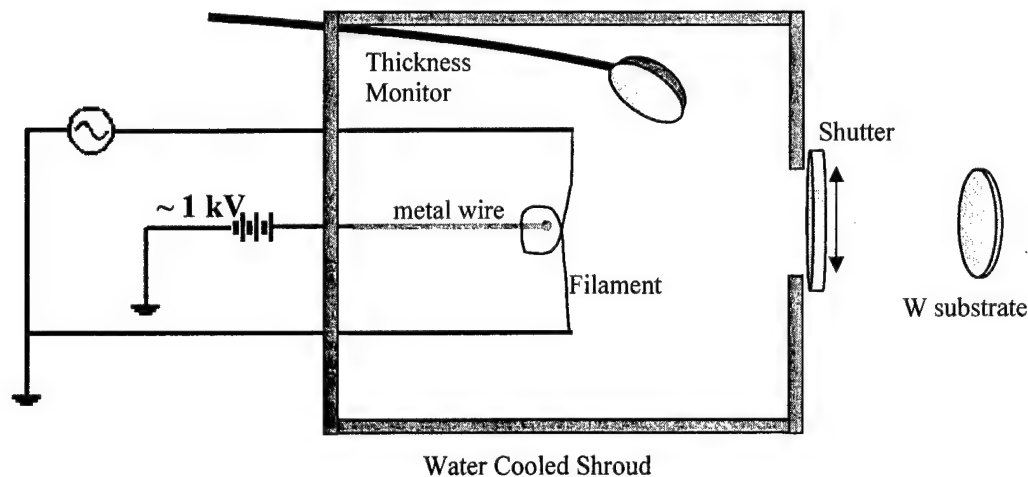


Figure 6: Diagram of MBE Cell Along With Its Water Cooled Shroud and the Tungsten Substrate.

Finally, the most important thing to consider in the MBE cell is a way to position the metal wire and W filament in a consistent manner to produce a reliable calibration. The metal source wire is inserted into a cylindrical holder with a small set screw to hold it in place. Both ends of the W filament are held in place by inserting them into a narrow hole and tightening a set screw. Originally, a 0.015" W wire filament was used. However, when a current close to evaporation conditions was passed through the filament it would deform and often short itself out on the source. Since the filament was deforming in the coils itself, simply bracing the ends of the filament would not help. So, 0.020" W wire was used for the filament. It was discovered that a Phillips-2 screwdriver shaft (0.250" diameter) made an excellent tool for a consistent filament geometry. Two full wraps were taken around the screwdriver shaft with the W wire. Then, the

filament could be put into place. This ensured well shaped, tight, and consistently placed loops of filament wire (diameter $\sim 0.265''$). Figure 7 is a front view of the MBE cell with the collector removed, showing a close up view of the filament and source wire.

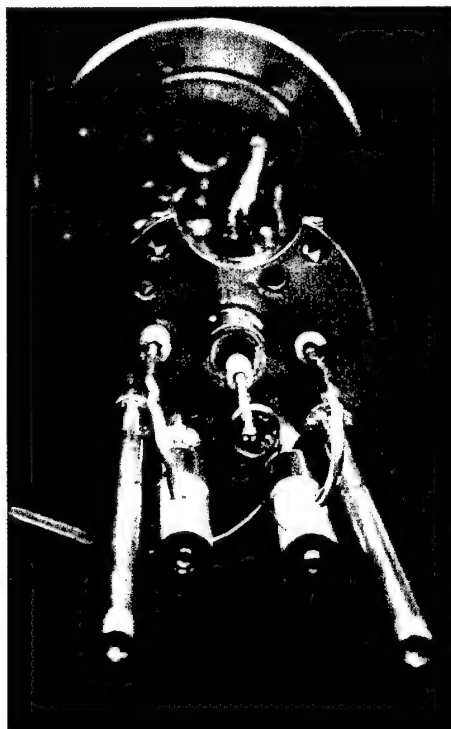


Figure 7: The tungsten filament and iron source can clearly be seen in this photograph of the MBE cell with the collector removed. Both copper wires running parallel to the source and supplying current to the filament have been completely covered with evaporated metal.

SAMPLE HOLDER

The sample holder and manipulator installed in the CMA system was in excellent condition and only a few adjustments were needed in order to prepare it for evaporations. The sample holder allowed rotation of the sample through a full

360°, tilting of the sample around a position perpendicular to the ground, and adjustments of the sample in the x, y, and z directions.

Where the sample attaches to the sample holder, the holder must be constructed out of high melting point metals such as molybdenum ($T_{\text{melt}} = 2617$ °C), tantalum ($T_{\text{melt}} = 2996$ °C), and tungsten ($T_{\text{melt}} = 3400$ °C). This is because the sample holder must be able to withstand the high temperature flash of the substrate. Holes were machined into a ring shaped piece of molybdenum to allow for easy attachment of the substrate. Using a W substrate with holes machined in it as well allows it to be lashed to the sample holder with 0.005" tungsten wire.

Similar to the MBE cell, the sample holder provides a means for raising the sample to a high voltage (1 – 2 kV) and passing a current of several amps through a filament in close proximity to the substrate. Once again, care must be taken to ensure the different components are electrically isolated from each other. The filament is made out of tungsten wire with a diameter of 0.020" wrapped into a three or four turn coil. Both ends of the filament are held in metal cylinders with set screws. Care should be taken so that the filament does not exceed a distance of 0.25" from the substrate or it will not be effective. At the same time, the filament should not be placed too close to the sample or they could come into contact and cause a short circuit. There is a small amount of play in the filament and the author has bumped the sample manipulator putting it into the vacuum chamber and caused a short at least once. Figure 8 shows the proper geometry for the filament when placed behind the tungsten substrate.

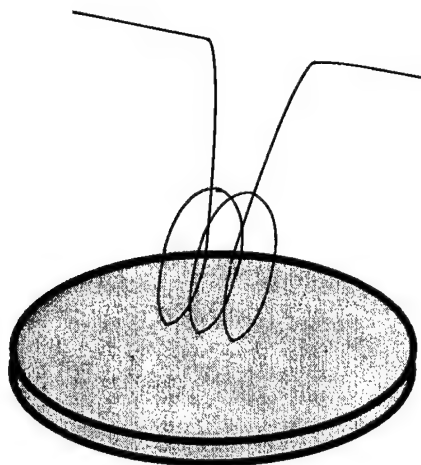


Figure 8: Filament shape and positioning behind the tungsten substrate that allowed the sample to be flashed consistently.⁴

Once any work is completed on the MBE cell, sample holder, or any other piece of equipment that will be inside the vacuum chamber, it is necessary to clean it with acetone. This will remove most contaminants that the items received through handling and will pay off later when trying to achieve a good system pressure.

MBE CELL AND SUBSTRATE POWER SUPPLIES

Power supplies are needed to supply the high voltages and currents necessary for evaporation and high temperature flash. These power supplies were built in-house by past researchers in our lab. A number of modifications and upgrades were necessary before these power supplies could be used.

The evaporator and sample power supplies are nearly identical. They are both capable of supplying over 20 A of current to their respective filaments as well biasing either the metal wire or substrate by several kilovolts (DC). Two

meters are used by both power supplies. The meter on the supplies' left side (when viewed from the front) measures the voltage applied to the source/sample and can also measure the emission current by toggling a switch. Emission current is generated by the electrons from the filament bombarding the biased source/substrate. Monitoring the emission current is a useful tool for determining how much power is being put into the wire/substrate (and therefore the amount of heating) and is related to the evaporation rate of the metal source wire in the MBE cell. Directly below this meter is the variac which controls the HV supplied to the source/substrate. The meter on the supplies' right side monitors the filament current. Directly below this meter is the variac which controls the filament current. On the supplies' far left side are the master power switch and switches that turn the HV and filament current on/off. Figure 9 shows the front of the upgraded evaporator power supply and Figure 10 is its block diagram.

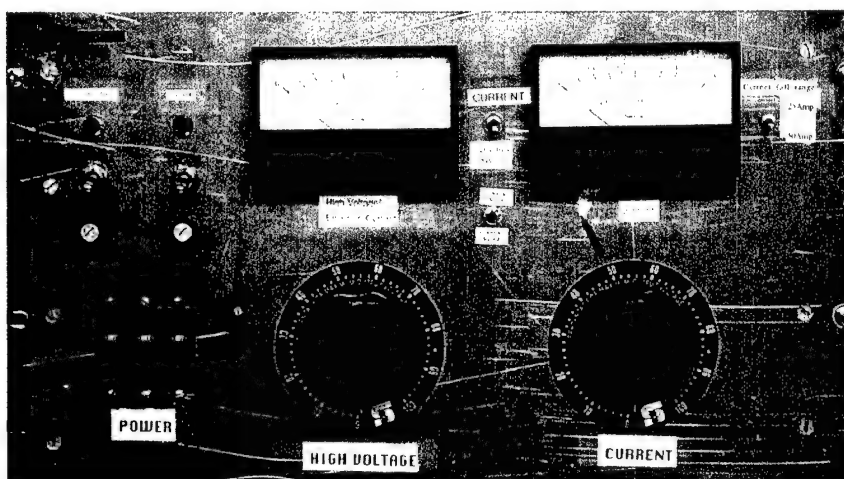


Figure 9: Front Panel of the Evaporator Power Supply. The sample power supply's front panel is almost identical except that it does not have the extra switch in the middle of the panel to toggle the emission current meter between two different settings.

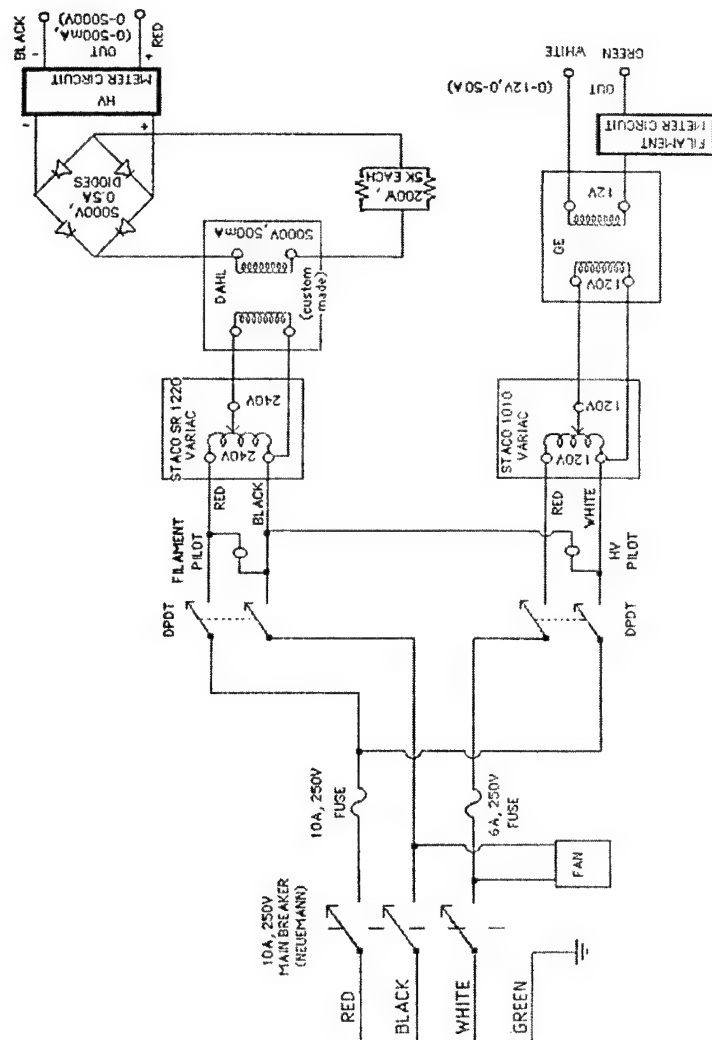


Figure 10: Block Diagram of Evaporator Power Supply. The sample power supply is identical.

Both power supplies provided HV, filament current, and monitored the filament current accurately when this project was started. However, the HV/emission current meters did not function properly. There were no reliable circuit diagrams for the meter circuits so the electronics had to be traced over, troubleshooting had to be done, and once a number of modifications were made new reliable circuit diagrams needed to be drawn.

The HV meter samples the voltages sent to the power supplies' MHV and BNC connectors through a basic voltage divider circuit. Once they were modified, both power supplies used the same circuit to measure the HV. For safety, two fuses are in series before the HV reaches either the connectors or the voltage divider. A $1\text{ M}\Omega$ resistor is the first element of the voltage divider. Next, a $100\ \Omega$ resistor is in parallel with a $25\text{ k}\Omega$ potentiometer that is series with a Simpson $50\ \mu\text{A}$ meter. Both the $100\ \Omega$ resistor and meter are grounded. Once completed, the HV meter circuit was calibrated by connecting the power supply to a $10\text{ k}\Omega$ resistor and monitoring the current through the resistor with a multimeter. The output voltage was adjusted until 0.100 A was measured with the multimeter. Then, the potentiometer could be adjusted until 1 kV was registered on the meter. When calibrated correctly, the meter can read voltages between $0 - 5\text{ kV}$.

A Double Pole Single Throw (DPST) switch allows the meter to be toggled between monitoring HV and emission current. Throwing the switch changes the contacts of the Simpson meter. When measuring emission current, electrons are accelerated from the grounded filament to the biased source wire or substrate. From there they pass through HV- on their way to ground. Between

HV- and ground there is a current divider. In the case of the sample power supply, a $1/3 \Omega$ resistor is in parallel with a 100Ω potentiometer that is in series with the Simpson meter. Both the Simpson meter and $1/3 \Omega$ resistor are connected to ground. The emission current circuit was calibrated by hooking up and Hewlett Packard power supply to the circuit and passing a known current through the circuit. By adjusting the 100Ω potentiometer the meter was calibrated to measure emission currents from 0 – 500 mA.

The emission current meter circuit for the evaporator operates on the same principle but has a few minor changes. When growing films in the CMA system, the emission current between the filament and wire does not exceed 50 mA. So, a range of 0 – 50 mA was desired in addition to the 0 – 500 mA range. An additional DPST switch was added to the supply's front panel. A 3Ω resistor replaced the $1/3 \Omega$ resistor in the circuit and the switch allowed an additional $1/3 \Omega$ resistor to be toggled in and of the circuit, in parallel with the 3Ω resistor. This way, the supply was able to measure the emission current over two different ranges. The same method was used for calibrating this circuit as the sample power supply.

A few additional modifications were made to the power supplies. As an example, a number of components were grounded on the chassis front panel. For safety reasons, these components are now grounded at the back of the chassis. Cables needed to be built to supply the HV and currents from the power supplies to the MBE cell and sample in the vacuum chamber. These cables were easily manufactured in the lab. Circuit diagrams of the HV/emission meter circuits for

the evaporator and substrate power supplies are displayed in Figures 11 and 12. As an additional note, the evaporator power supply requires that the filament be connected to the chassis ground using an external connection on the back of the supply's chassis. This completes the emission current circuit.

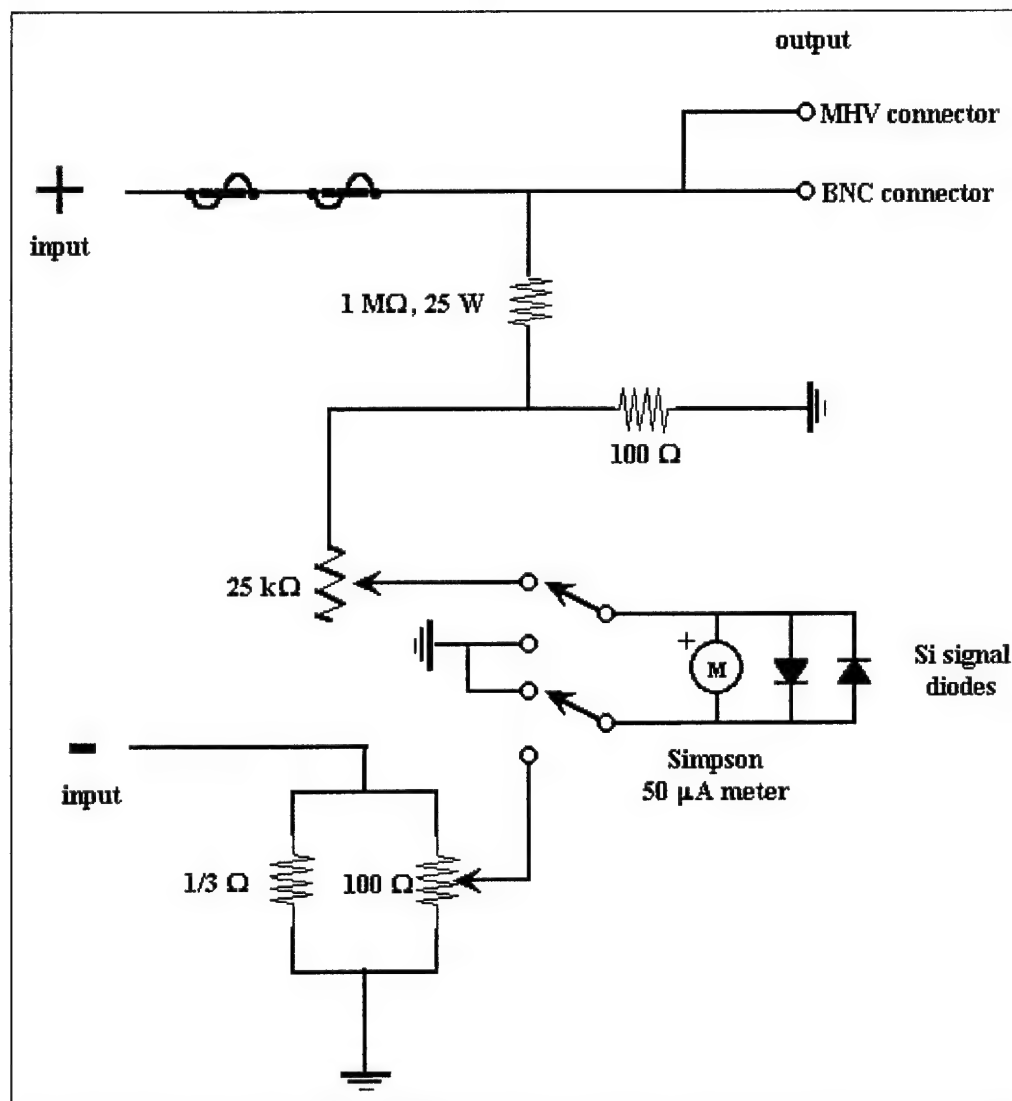


Figure 11: Substrate Power Supply HV/Emission Meter Circuit.

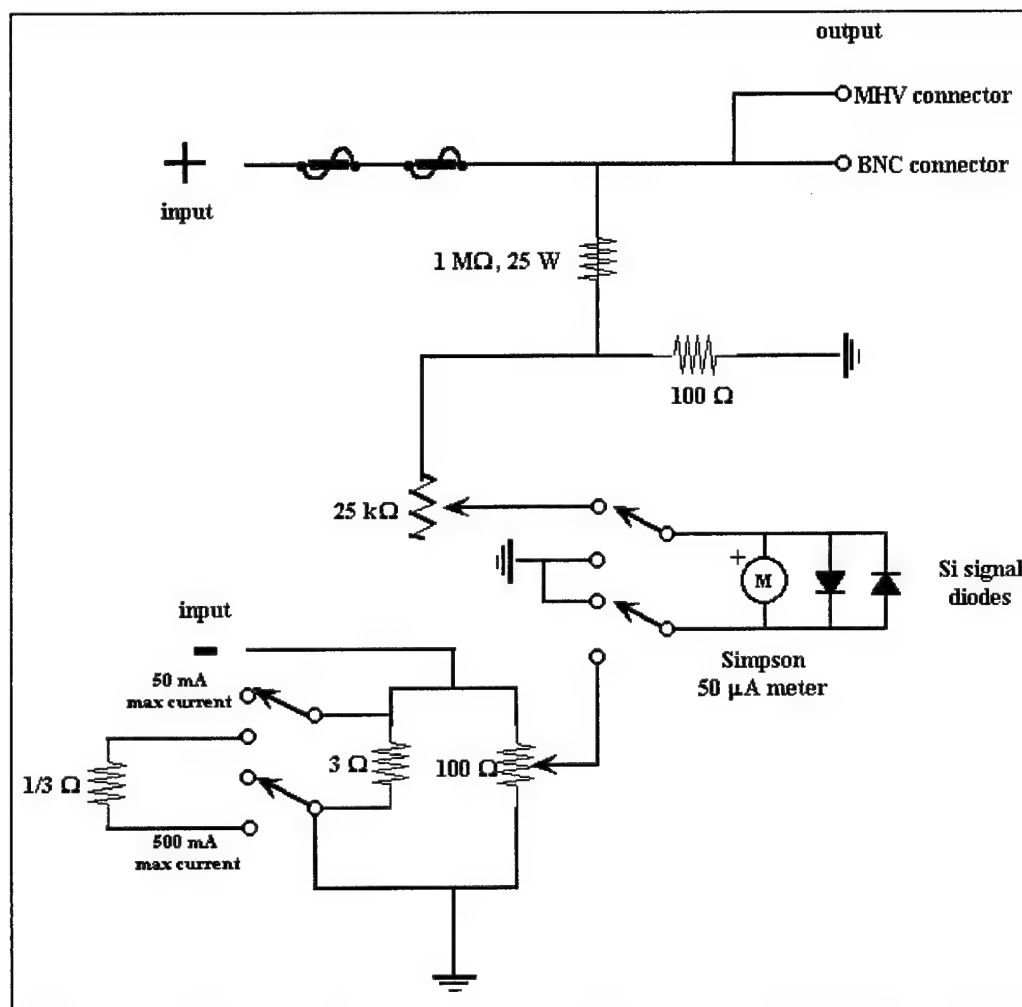


Figure 12: Evaporator Power Supply HV/Emission Meter Circuit. The circuit which measures the emission current has the added feature of two settings: 50mA max. deflection and 500 mA max. deflection.

BAKE-OUT ELECTRONICS

When trying to achieve system pressures in the 10^{-10} Torr range, the vacuum chamber must be baked. During baking the stainless steel walls of the vacuum chamber are raised to temperatures between 100 – 150 °C. This causes many of the contaminants that have adsorbed to the walls of the chamber to be desorbed and removed by the system vacuum pumps. Resistive heating bands are placed at various locations on the vacuum chamber. Other parts of the vacuum chamber are heated by radiative heating elements. Alternating current is supplied to these heating elements from 220 VAC wall outlets in our lab. This heating process must be controlled by a bake-out control box built in-house.

It is vital that the temperature does not exceed the desired level during bake-out. Extremely high temperatures could damage sensitive components and cause leaks to occur in copper gasket seals. However, the temperature should not drop too low or the bake-out will be ineffective. The entire vacuum chamber is divided into four regions in which the temperature is controlled separately. It will be helpful to reference Figure 2 to see the regions of the vacuum chamber. The regions are the bell jar (the portion of the system visible above the rectangular base), chamber and pump (both of which are within the rectangular base), and turbo (the section connected to the turbomolecular pump which can be seen to the left of the rectangular base).

In order to maintain the proper temperature, each region of the system is fitted with a thermal switch. This thermal switch is connected to a -15 V (DC) supply on one end and to a solid state relay on the other. The solid state relay is

also connected to a switch on the front panel which allows the bake for each region to be turned on or off. When the front panel switch is closed, +15 V (DC) is supplied to the solid state relay. So, when both the front panel and the thermal switch are closed, 30 V are supplied to the relay, turning it on and allowing the 220 VAC connected to its other contacts to power the heating elements. So, if the front panel switch is turned on and a region reaches too high of a temperature, the thermal switch opens and stops the bake for that region. Once that region drops back within an acceptable temperature, the thermal switch closes again and the bake resumes. Neon light bulbs above the front panel switches light up when a particular region is baking. As an additional note: the bake-out electronics box also has a fifth auxiliary switch capable of supplying power to an additional heating element if necessary.

A number of upgrades and repairs were made to the bake-out electronics during this project. Many of the circuits wouldn't heat their respective regions properly and many of the neon lights did not operate as they should. First, a number of the solid state relays no longer worked and had to be replaced. Also, several the neon bulbs were found to be wired incorrectly or had to be replaced. These repairs allowed the system to operate as designed.

However, there were still a number of poor design issues that needed to be corrected and some upgrades that needed to be made while the chassis was opened. As an example, for no logical reason there were two master power switches on the chassis front panel. Once all the upgrades were made, a reliable circuit diagram needed to be drawn.

We wished that the bake-out process could be switched between two modes: ion pump and turbo pump. The turbo pump mode would be used when the system was only being pumped by the fore-pump (also known as the roughing pump) and the turbomolecular pump. In this mode, the electronics use 110 VAC split off from the 220 VAC wall outlet power. The ion pump mode is selected when the ion pump is being used in conjunction with the other two pumps during the bake process. This setting takes advantage of the auxiliary power supplied by the ion pump while it is running. As long as the ion pump is on, 110 VAC is supplied. This acts as a safety measure since if the system pressure increases too much (as when a leak occurs), the ion pump automatically shuts off as long as it is set in the protect mode (vs. start mode). The ion pump shutting off would automatically shut off the bake-out so a leak would not continue to be aggravated by the elevated temperatures. Since a system is often left to bake overnight or over a weekend, this is an excellent feature which can be engaged with a simple switch.

No matter which source the 110 VAC comes from, it is routed to a relay's magnetic coils (terminals 7 and 2 – see Figure 13) through a 24 hr. timer. The timer has a Time Delayed Open (TDO) switch. As long as the timer is on and counting the switch remains closed and 110 VAC is provided to the relay. Once the timer runs out, the switch opens and current is no longer supplied to the relay. Next, the system was given one master on/off switch. When the master switch is turned on, it supplies 110 VAC to the relay's inputs (terminals 1 and 8) and a

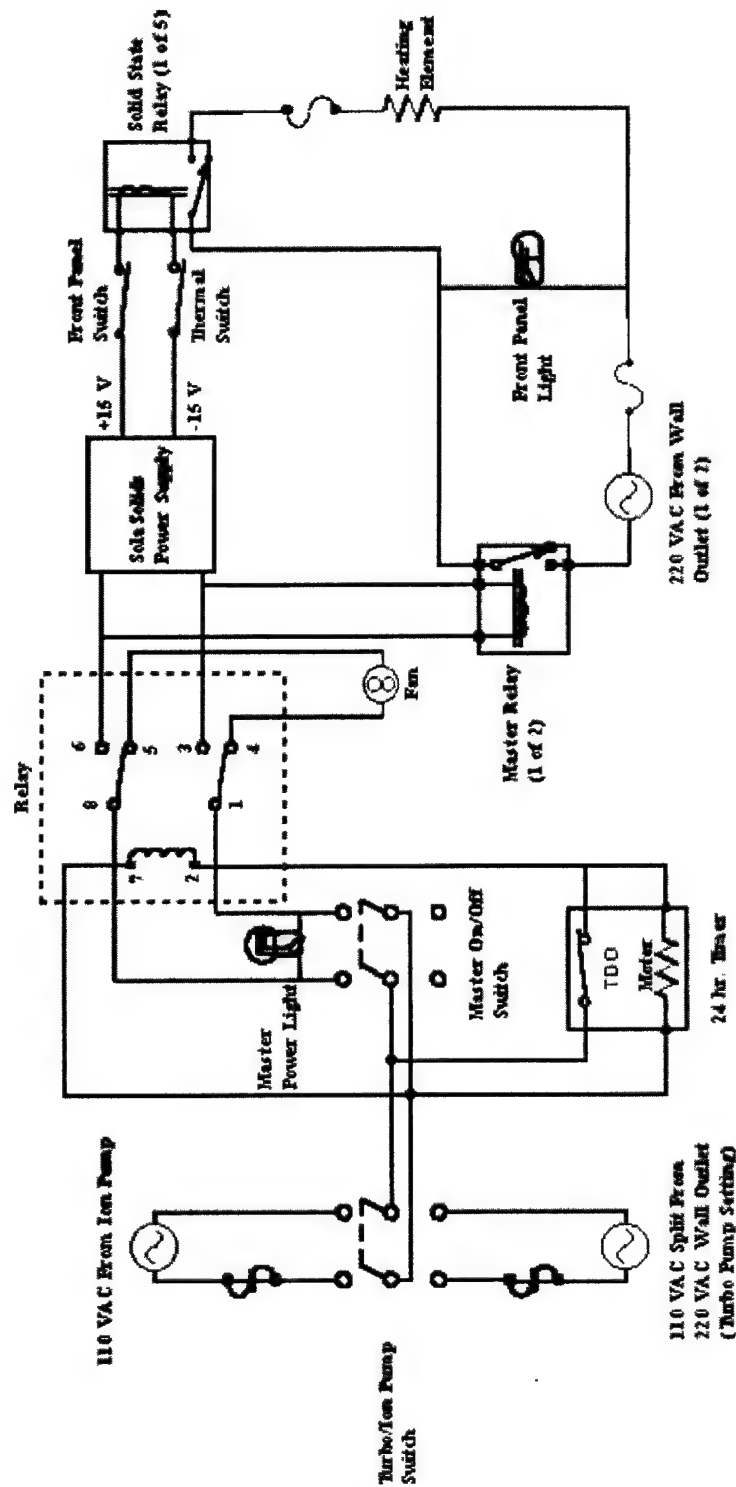


Figure 13: Upgraded Bake-Out Electronics. In the actual circuit, there would be an additional 220 VAC wall plug connected to a second master relay. One 220 VAC plug/relay combination would be connected to three solid state relays and power three heating elements, while the additional plug/relay combination would be connected to the remaining two solid state relays.

neon light which serves as an indicator. The front panel with the single master on/off switch as well as the ion/turbo pump switch is displayed in Figure 14.

In the relay's inactivated state (no current supplied to the magnetic coils), the inputs are in contact with terminals 4 and 5. Terminals 4 and 5 are connected to an output on the back of the bake-out electronics chassis. The power from this output can drive a fan on the rectangular base of the vacuum chamber. Our vacuum system does not currently have a fan but there are plans to install one. As long as the master power switch is on but the timer is off (no longer counting down) power could be supplied to a fan. This feature allows the fan to turn on once the bake is complete and cool the vacuum system more quickly.

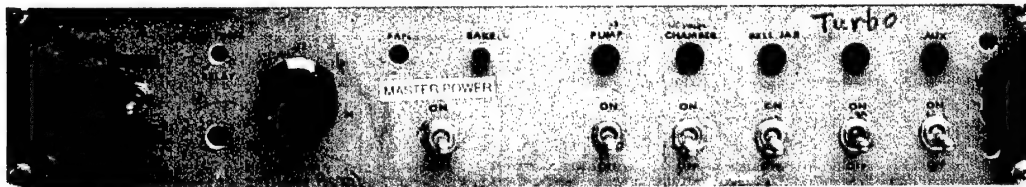


Figure 14: Front Panel of Upgraded Bake-Out Electronics.

When current is supplied to the relay's magnetic coils, the 110 VAC is diverted to terminals 3 and 6. From here, 110 VAC is provided to two master mechanical relays. When 110 VAC is provided to these relays, they allow the 220 VAC from the wall outlet to continue to each of the five solid state relays. The 110 VAC also powers a Sola Solids Power Supply which provides ± 15 V DC to the thermal switch and solid state relay circuit discussed previously.

Chapter 4: Software Development

A large portion of this research project was devoted towards the development of software for the thin film growth system. Software was needed to record and integrate the ion current, record the crystal monitor output during an evaporation, and to record the output from the AES system during Auger analysis. It was decided that the most practical way of achieving this goal was by using a National Instruments (NI) Data Acquisition (DAQ) board and NI's Labview software.¹³ A PCI-6023E DAQ board was installed in a PC and attached via a NI cable to an NI CA-1000 enclosure which contained a standard breakout board.

Labview is a graphical programming language based on Virtual Instruments (VIs). VIs are essentially blocks of Labview code that can run as completely independent programs or perform subroutines within a larger and more complex VI. A Labview VI consists of a graphical user interface with graphs, displays, switches, etc. and the actual code which resembles a circuit diagram connecting all of the sub VIs via 'wires'. Labview is most often used as a data flow programming language. In other words, tasks are executed based on when data arrives to them. The combination of NI hardware and Labview software provides a straight forward way of integrating computer software and lab equipment.

MBE INSTRUMENTATION SOFTWARE

The first task was to develop software and hardware to monitor the MBE instrumentation. First, an interface with the Keithley picoammeter used to

monitor the ion current had to be developed.¹⁴ The picoammeter outputs $\pm 2\text{V}$ (analog) depending on the current that it is reading.¹⁵ The picoammeter was connected to one of the DAQ board analog channels via a BNC connection to the CA-1000. Labview was set up to accept a differential input in order to minimize noise.

Once the picoammeter was interfaced, the software was developed by starting with one of the example VIs for buffered analog input. The examples provided within Labview are very robust and make an excellent starting point. A buffered input was chosen since it provides the most accurate timing possible with Labview (unless you drive the system with an external trigger). A while loop contains the entire acquisition process and can be terminated by pressing a stop button on the user interface. The data is gathered in a waveform format at a rate of 1 Hz (the acquisition rate can be configured on the user interface panel). Data values and the time between samples (dt) are then extracted from the waveform. At the time of acquisition, the data values are sent to both an output on the user interface and to a shift register. A shift register allows data values from previous iterations of a loop to be used in the current iteration. The shift register was very useful for building an array of all the ion meter values throughout an acquisition. This array, along with the dt values, is sent to a sub VI which calculates the integrated ion current.

A particularly challenging part of developing the MBE VI was interfacing to the Inficon thickness monitor. The thickness monitor in our lab dates back to the 1970's and has a female 9-pin serial port connector (RS 232) to allow communication with a PC. After many tries to communicate with this instrument via the PC's serial port it was finally discovered that the serial port pin outs on the XTC do not match the standard pin outs used today.¹⁶ To remedy this problem, a RS 232 cable had to be modified to match the PC pin outs to those of the XTC. Figure 15 shows the standard labeling of a female 9-pin RS-232 connector and Table 1 lists the function of each pin on the XTC. As a special note: only the XTC controllers with a 'G2' in the serial number have the ability to communicate via a serial port although all XTC controllers have a serial connector.

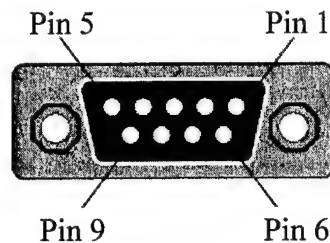


Figure 15: Female 9-Pin RS 232 Connector Used On XTC.

RS 232 Pin #	Pin Function
4	Transmit
5	Receive
1, 2, 6	Ground

Table 1: Pin Functions of XTC RS 232 Connector.¹⁶

With the RS 232 problem resolved, the rest of the interfacing could proceed. Once again, an example VI for serial communication was used as the starting point. In order to achieve the timing necessary for serial communication this VI could not rely simply on data flow programming. Instead, a programming structure called a sequence loop was used. A sequence loop can be made up of any number of frames which are executed in order. The VI will not move on to the next frame until all of the tasks in the previous frame are completed. Four sequences make up the VI that communicates with the XTC and execute the following tasks: initialization, write data to the XTC, wait for a specified time, and read data from the XTC.

The ASCII 'D' followed by an ASCII acknowledge (6) is sent to prompt the XTC to transmit its elapsed time, thickness, and deposition rate.¹⁶ Once the message is sent in the write the data sequence, the VI waits for a 500 ms delay and then reads the XTC output over the serial line during the last sequence. When the data are acquired in string format, various manipulations of it using Labview's many string related VIs are performed to display the data in a user friendly and

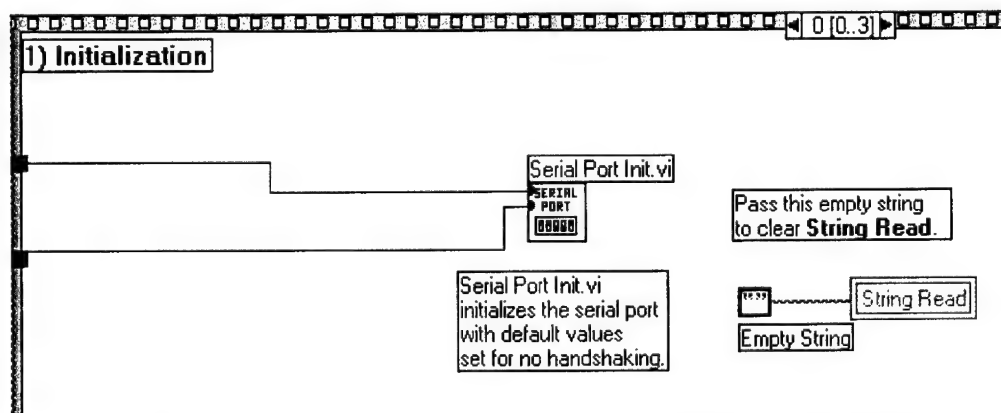


Figure 16: Initialization Sequence (1 of 4) of XTC VI. The rest of this sequence only contained empty space and was omitted from the figure.

input. Finally, the timing of the system was not achieving a 1 Hz repetition rate until all operations were integrated under a single while loop (an effect of data flow programming). The user interface of the MBE VI is displayed in Figure 20 and the “circuit” diagram is displayed in Figure 21.

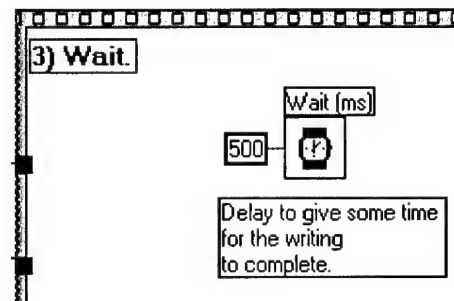


Figure 18: Wait Sequence (3 of 4) of XTC VI. The rest of this sequence only contained empty space and was omitted from the figure.

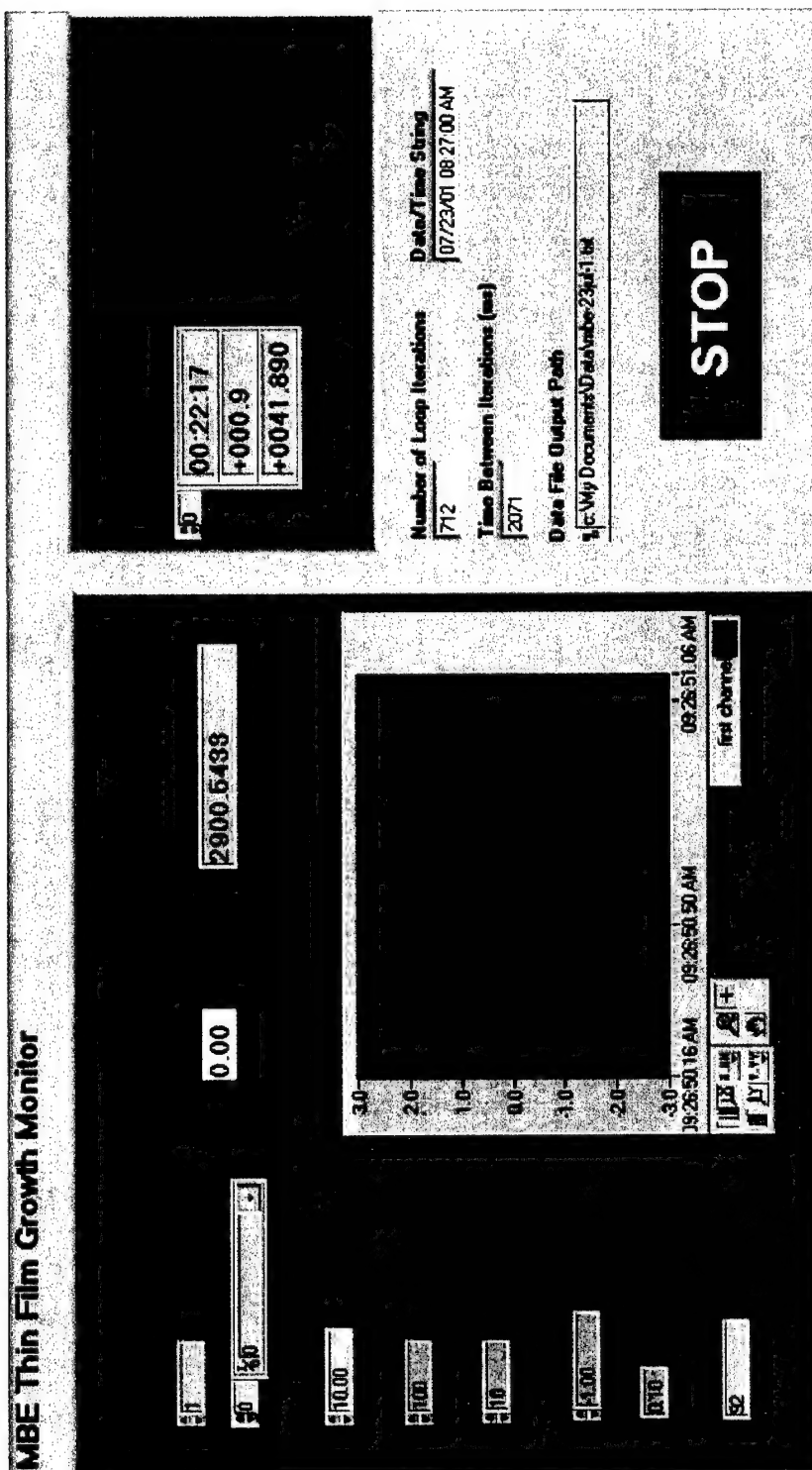


Figure 20: User Interface of MBE VI.

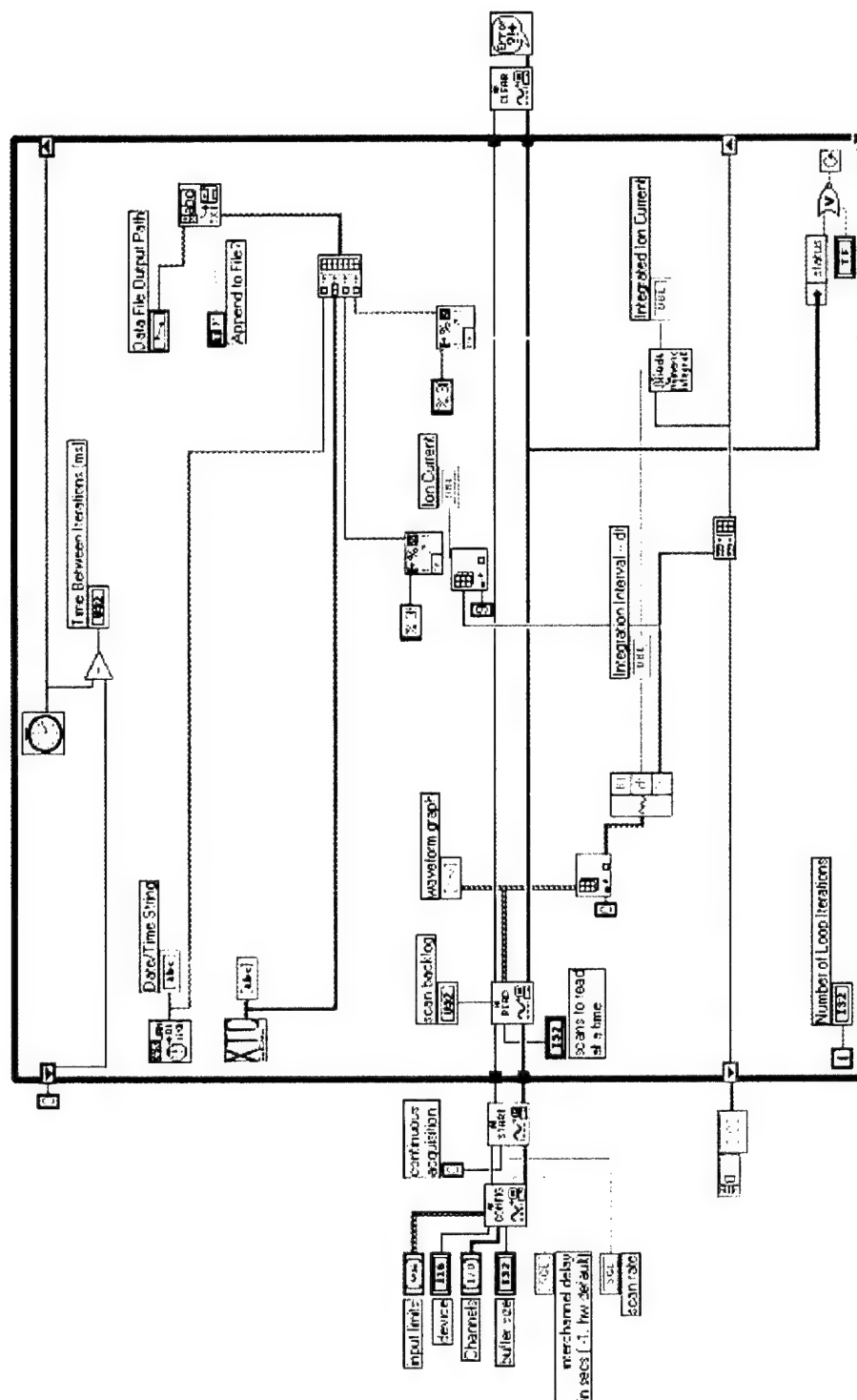


Figure 21: 'Circuit' Diagram of MBE VI.

AUGER ELECTRON SPECTROSCOPY SOFTWARE

Next, the software to display Auger spectra was written. Although this task had its challenges, it did not prove to be nearly as difficult as programming the MBE VI. When this project was began, all of our lab's AES systems outputted their results to a pen and paper plotter. This could present a problem if the pen dried up during an acquisition or simply moved out of contact with the paper. Also, the mechanical plotter scale had to be adjusted every time a change was made to one of the AES settings. Finally, the power of having data in an electronic format which can easily be manipulated and saved in various formats cannot be understated.

The Auger system outputs two voltages simultaneously to BNC connectors for plotting. The voltages represent the energy in eV (x-axis) and the value of $dN(E)/dE$ (y-axis). Once again, an example VI for buffered data acquisition was used as a starting point. The entire VI is contained within one while loop which can be stopped from the control panel. This time, the data are read as a 2-D array of numbers during the data acquisition process. Data for each axis were collected at a rate of 10 Hz and every ten values (per axis) are averaged using a sub VI that finds the mean of an array of numbers. Averaging is used as a method of reducing noise.

Since the values for the x-axis are not the actual values in eV but rather a ramped voltage, several trial runs had to be performed in order to develop a calibration. The ramp voltage was linear so a calibration could be performed on the x-axis data using a simple slope and offset equation (Labview has a formula

box to perform such calculations). A shift register was used to pass data from previous iterations of the while loop to the current iteration and build an array of all the x and y values. This array continually updates an x-y graph in pseudo real-time. Finally, during every iteration of the loop the values are outputted to a data file in tab delimited format. This file can also be opened from any spreadsheet program so that the data can be plotted and manipulated. The user interface with a sample spectrum is displayed in Figure 22 and the “circuit” diagram is shown in Figure 23.

Auger Plotter

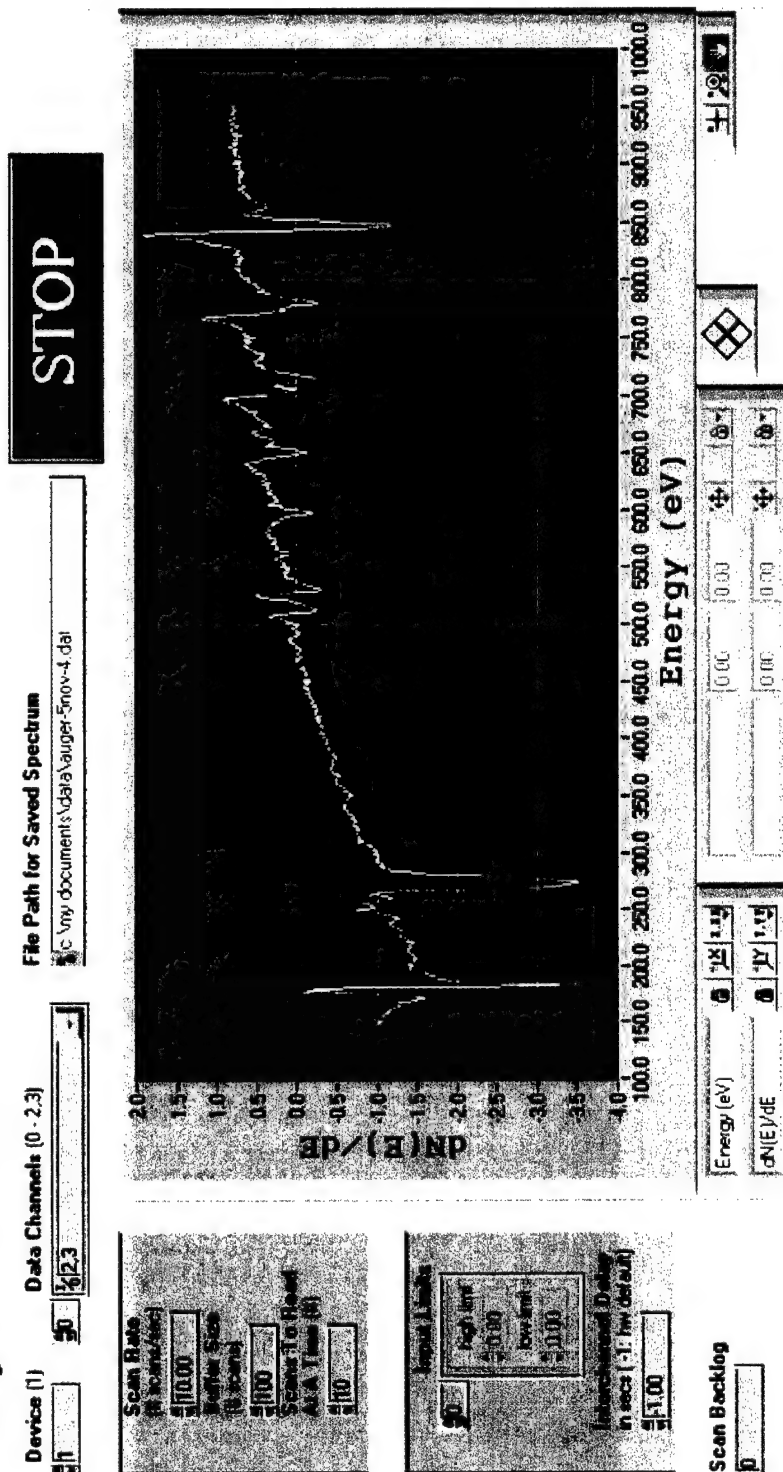


Figure 22: User Interface of Auger Plotter VI with Auger Spectrum Displayed.

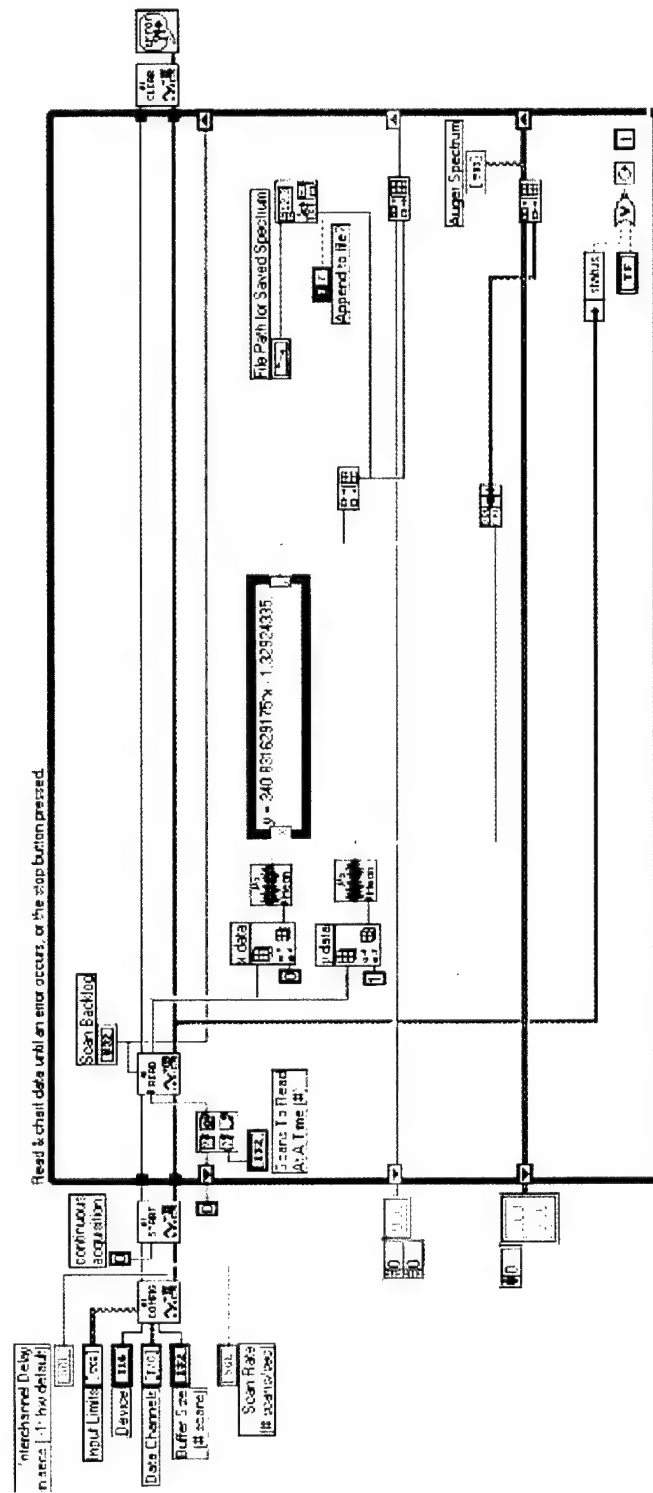


Figure 23: 'Circuit' Diagram of Auger Plotter VI.

Chapter 5: Preparation For Thin Film Growth

ACHIEVING UHV

With the necessary upgrades made and all instrumentation working, the system could be put under vacuum. It is necessary to grow thin films in UHV to reduce the amount of contamination. Gases present in the vacuum chamber can adsorb, or attach, themselves to any surface, including the metal source wire and the substrate. As an example, at an oxygen partial pressure of 1×10^{-6} Torr any surface in the vacuum chamber will have a full monolayer of oxygen adsorbates in one second.⁴

In order to achieve pressures in the UHV range (10^{-10} Torr or less) a series of pumps are used. First, a mechanical fore-pump or roughing pump is used to reduce the system pressure into the 10^{-3} Torr region. Once a pressure of 10^{-3} Torr is achieved a turbomolecular (turbo) pump can assist the roughing pump bring the system to a pressure of 10^{-7} Torr. Finally, an ion pump lowers the system pressure to the 10^{-10} Torr region and is used for long term pumping. It is possible to reach lower pressures using additional pumps (titanium sublimator) but for the purposes of this project it was not necessary.

Unfortunately, achieving UHV is not as simple as using the various pumps available for several hours. A bake-out process is necessary to desorb various contaminants including hydrocarbons, nitrogen, oxygen, and water. Otherwise, the pressure will never get out of the $10^{-8} - 10^{-9}$ Torr range. Once the contaminants desorb from the walls of the chamber during bake-out, they are removed by the system pumps.

For the CMA chamber a standard method used in our lab worked well for achieving UHV pressures. First, the system is pumped down using the roughing pump for at least an hour, at which time the turbo pump can be turned on. After approximately 24 hrs., the system will reach a pressure in the 10^{-7} Torr range. It is at this point that the researcher can feel confident that no leaks are present and start the bake-out process. If a quick turnaround is needed, it is possible to bake the system after pumping for less than a day, but the ion pump shouldn't be turned on until the system has reached a pressure near 10^{-7} Torr.

Next, the system is wrapped in heavy-duty aluminum foil and the bake electronics are turned on. It is important to note that the valve between the bell jar and the turbo pump is not bakeable and must remain open while baking. A bake-out can last a minimum of 12 hours or up to several days (often over a weekend). During the initial portion of the bake-out, the pressure will rise but will then begin to lower gradually. Once the pressure returns to the 10^{-7} Torr range and has been baked for several hours the ion pump can be turned on. After the ion pump's initial startup and when its pressure gauge begins reading 10^{-5} Torr or less it is wise to switch the ion pump into protect mode. This will prevent the ion pump from continuing to pump if the system has a leak and potentially shorten its lifetime.

During the last 4 – 12 hours of a bake it is a good idea to outgas the filaments, substrate, and metal wire. This removes any contaminants that have adsorbed to them, helps the system achieve lower pressures, and also prevents large spikes in system pressure during an evaporation or high temperature flash.

When outgassing the source wire and its filament it is important to remain below the evaporation threshold and not pass a current through the filament that it will not be able to withstand for several hours. For the CMA chamber with our geometry it was found that a current of 10 – 11 A in the filament coupled with biasing the wire by + 1.2 kV worked best. When outgassing the W substrate and its filament, a temperature of 600 °C is desired. It was found that this temperature was best achieved by biasing the crystal at +1 kV and passing 9 A of current through the filament. The 600 °C temperature was verified by a pyrometer.¹⁷

It is very important to verify that the knobs that control both the filament current and the bias voltage are turned all the way off before turning on the substrate and evaporator power supplies. If the filament current is set to a high enough level, the sudden increase in current can blow out the filament. This means a minimum of three down days in order to vent the system, replace the filament, and return the system to UHV.

If the system has baked for at least 12 hrs. and the pressure is in the 10^{-7} Torr range, the bake can be ended. If possible, it is best to turn the bake off and let the vacuum chamber begin to cool before stopping the outgassing process so that the filaments, substrate, and metal wire will have as few adsorbates as possible. Once the system is cool enough to touch with a bare hand, the valve between the bell jar and the turbo pump can be closed and the turbo pump can be turned off. A pressure of approximately 2×10^{-10} Torr should be achieved as the system cools off.

HIGH TEMPERATURE FLASH

Before beginning film growth, it is important to be sure that the substrate is clean. So, the W crystal has to be flashed as discussed earlier in order to ensure that the crystal is clean of impurities. A crystal temperature between 1800 and 2100 °C is desired when flashing. Of course, care must be taken not to raise the crystal to higher temperatures due to the danger of a local melt.

After flashing the crystal many times, settings for the filament current and substrate bias voltage that worked well for this chamber and setup were determined. First, the W crystal is biased at +1.5 kV and the filament current is slowly raised to 12.5 A. The electron flux onto the substrate will decrease the bias voltage. So, in order to raise the temperature to the proper level the voltage is increased back to approximately 1.5 kV. The emission current can also be monitored since it is directly proportional to the heating of the crystal. Emission currents typical during a flash are approximately 65 mA. This produces a crystal with a temperature between 1800 – 1900 °C.

When flashing properly, the crystal is heated until it is white hot or appears to resemble a “mini-sun.”⁴ Since it is not wise to look at the crystal with the naked eye during the flashing process, a pyrometer can be used to verify the crystal temperature. Once the proper flashing temperature is reached, it is held for 20 seconds. At the completion of the flash both the bias voltage and filament current are decreased to zero. It is a good practice to make sure that the mechanical shutters that cover the LEED and AES are in place to protect them from having any material deposited on them during the flash.

Further cleaning of the crystal is still possible. For example, even the purest commercially available metals have some amount of carbon in them. This carbon can be removed through a process called annealing. However, for the purposes of this project it was not necessary. Once the crystal is flashed, its cleanliness must be verified.

AUGER ELECTRON SPECTROSCOPY

Numerous Auger spectra were taken as part of this research project. Over time, the settings that worked best for this particular system and setup in conjunction with the Labview software were worked out. The sample manipulator allows precise positioning of the sample within the vacuum chamber. If the positive z direction is taken to be along the axis of the sample manipulator and pointing towards the ceiling, there are two micrometers that allow positioning of the sample in the x and y directions. The x-axis micrometer was set to 0.0400" (in the black lettering) and the y-axis micrometer to 0.0585" (black lettering). There are no indicators for setting the sample height in the z direction. So, the height was adjusted until the sample appears to be lined up with the AES aperture. Rotation about the z-axis is also allowed by the sample manipulator. For taking Auger spectra, the manipulator was set to 194°.

A picoammeter or electrometer can be used to measure the target current (current from the e-beam bombarding the substrate). For the settings used during this project, typical target currents were 5 – 15 μA . The target current should only be checked during preparation for taking Auger spectra since the sample must be grounded during the actual measurements. If the substrate is not

grounded, inaccurate Auger spectra will result due to a buildup of charge. Although the picoammeter provides a path to ground for the bombarding electrons, it has a high enough resistance to allow some buildup of charge on the substrate. Therefore, the best course of action is to short the sample to ground. There are various other settings that can be adjusted on the rack mounted AES electronics. The settings used during this project are outlined in Table 2.

AES Electronics Setting	Value
Electron Gun Bean Voltage	3 kV
Electron Gun Emission Current	1.2 mA
Analyzer Control Modulation	2 V peak-peak
Lockin Amplifier Gain	200x
Lockin Amplifier Time Constant	0.3 s
Lockin Amplifier Phase	20°
Electron Multiplier Supply Channel Voltage	1500 V

Table 2: Auger Control Settings That Worked Well For the CMA System

Care must be taken when setting the electron gun current to ensure a long life for the filament. Start with the emission set to its maximum level and begin raising the filament current. It takes approximately seven full turns of the filament knob before the meter shows a response. Once some filament current is registered, the emission should be reduced slightly. When turning off the electron gun follow the same steps but in reverse. Importantly, the electron gun emission

current must be watched and adjusted regularly with the filament current knob since it has a tendency to creep higher during operation. To preserve the filament's lifetime and avoid breakage, the emission should never exceed 2 mA.

Although the Auger spectra for this system is recorded digitally, the rack mounted AES plotter is still a useful tool. The plotter allows the AES system to be fine tuned through examination of the elastic peak. By setting the energy of the electron gun to 0.5 kV, the elastic peak can be found by manually slewing the AES system. This way, the focus and x and y steering on the AES electronics can be fine tuned, maximizing the response to the elastic peak. Typically, both coarse and fine focus knobs were turned fully in the counter-clockwise direction during our experiments.

Chapter 6: Evaporations

A considerable amount of this project was devoted to learning the best methods for film growth with the CMA chamber. Some members of our lab go as far as to consider thin film growth an art. After many trials and errors, a system that works well for the CMA chamber was developed.

First, the substrate must be positioned facing towards the MBE cell, which corresponds to setting the sample manipulator to 83° . The x, y, and z positions of the sample are left on the same settings as those used for taking Auger spectra. This places the sample a distance of 7.375" from the source wire tip, when the tip is in line with the filament.

Before starting the evaporation, the water cooling for the MBE shroud and XTC crystal is turned on and allowed to circulate for about 5 minutes to allow everything to come into thermal equilibrium. The values of the source density and z-ratio (acoustic impedance ratio which takes into account the shear moduli of both the deposited film and the quartz crystal) must be inputted into the XTC control electronics.¹⁶ These values can be looked up in a table in the Inficon user manual. For an alloy such as permalloy, a weighted averaged for all of the elements in the alloy is used to determine the proper density and z-ratio values. Once the water cooling has been on for 5 minutes, the XTC display can be zeroed.

Evaporations are started with the shutter to the MBE cell closed. Originally, the shutter was left open throughout the entire process but after several

trials and discussions with other researchers it was decided to keep the shutter closed until the proper evaporation conditions are reached. Just as when flashing the substrate, it is wise to keep the LEED and AES shutters closed to protect them from material deposition.

Next, the evaporator undergoes a soak period. During this time, the wire tip is heated to a temperature that is below the evaporation temperature. This allows the wire tip to outgas and the MBE cell and crystal monitor to come to thermal equilibrium at a temperature close to evaporation temperatures. Settings that worked well for soaking were a +1.2 kV bias voltage and 14 amps of filament current. This produced an emission current of approximately 5 mA. The most important setting to monitor is the emission current, since it is directly related to the amount of heating in the tip. Changes in the filament current are acceptable as long as the emission is maintained close to 5 mA. The soak conditions are held for 5 minutes. During this time, the rate and thickness values of the crystal monitor will experience a temperature drift and then stabilize at values offset from zero.

After completing the soak period, the temperature of the wire tip can be raised to evaporation temperatures. Threshold for evaporation occurs at 1.2 kV of bias voltage along with filament currents near 15 A. In the CMA system, the filament current was raised to approximately 16 A. Care must be taken that the filament current is not raised to near 20 A. Once currents of this level are passing through the filament, it is dangerously close to breaking. As stated earlier, a broken filament results in at least three lost days of research time.

When the threshold for evaporation is surpassed, very small changes in filament current can result in large fluctuations of emission current. For example, a change in filament current that is almost imperceptible in the power supply's meter can cause a 10 mA change in emission current. The emission current must be high enough to provide adequate heating to the wire tip for evaporation but not too high that it melts the tip and causes it to deform under its own weight. An example of a wire tip that was heated too much is shown in Figure 22. The Fe wire, with a diameter of 0.080", could be heated with up to 30 mA of emission current and not deform. However, this produced a high rate of growth and emission levels of 25 mA produced better results. The permalloy wire, with a diameter of 0.060" deformed when heated with an emission of only 25 mA. So, it must be heated with emission levels closer to 20 mA.

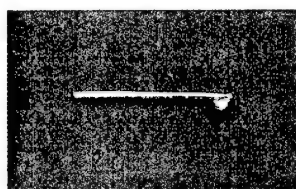


Figure 24: Permalloy Wire Heated Too Aggressively. When too much emission current was used to heat this wire, the portion of the tip that was melted became too large for its surface tension to hold it in place. The liquid permalloy then fell beneath the wire, leading to very poor evaporation efficiencies.

Once an emission current that safely provides a desired evaporation rate is chosen, it is important to monitor the emission current and maintain that level with small corrections in the filament current. Since the filament will rise to temperatures higher than those during the soak period the crystal monitor will again undergo a temperature drift. During the thermal drift, both the thickness

and the rate of deposition will become negative. Once evaporation begins, the crystal monitor will start registering positive values again. It is at this point that the MBE cell shutter is opened and the Labview MBE software is started. During the evaporation, the filament current is adjusted as necessary to maintain the desired emission. After evaporating for the desired amount of time (or after depositing the desired amount of material), the filament current and source bias are reduced to zero, the shutter closed, and the software stopped.

After several evaporations, the source will start receding from the filament as it is used up. There is no way to visually monitor this. However, if the filament current required to maintain the same level of emission starts increasing, it is a good indication that wire tip has receded too far from the filament. The wire should then be advanced until the filament current required to produce a set emission returns to the original levels. As a general guideline, five counter-clockwise turns of the knob controlling the linear motion feedthru advances the source tip 0.170".

Periodically, the source will be completely spent or other problems will arise which require venting the chamber and inspecting the MBE cell. It is necessary to work around the filament with care since it will be very brittle due to the heating it has undergone. Any rough treatment of the filament will cause it to break. The ceramic standoffs close to the source will accumulate a fair amount of deposited metal. This metal can be removed with a solution of acid before the standoffs become so heavily coated that they no longer act as insulators. Before returning the MBE cell to the vacuum chamber, a thorough check of all electrical

connections will prevent problems being discovered once the system has been lowered to UHV pressures three days later.

Chapter 7: Experimental Calibration

Calibration of the CMA thin film growth system could begin once reliable methods of film growth and taking Auger spectra were learned. Many short film growth evaporations (1 – 3 minutes) were carried out, followed by the collection of Auger spectra. During each evaporation, data from the crystal monitor and picoammeter monitoring the ion current were recorded. This data, coupled with the AES data, were used to calibrate the ion flux sensor.

Early calibration results were plagued by difficulties. It was not possible to completely cover the substrate with enough deposited metal so that the W peaks were not visible in the Auger spectra. The reason for this is uncertain. One possible cause of this could be islanding, where the deposited metal forms clusters, instead of depositing in even epitaxial layers. Another possibility is that some W from the MBE filament was being evaporated and deposited on the substrate. These early calibration runs were conducted at pressures in the 10^{-8} and 10^{-9} Torr range (the pressures achieved by the system without baking). When the system was baked and the pressures were lowered to the 10^{-10} Torr range, we were able to grow films that completely covered the W. Plus, another positive effect of lowering the system pressure was more efficient evaporation resulting from the improved e-beam heating of the source.

As stated earlier, the crystal monitor did experience a temperature induced drift in its readings, even though the crystal is water cooled. In an attempt to overcome this effect, a second crystal monitor was added in the bell jar

of the vacuum chamber, next to the substrate. Although this crystal monitor was not subject to a temperature drift, it was not sensitive enough to detect the flux levels incident at such a distance from the source either.

This project showed the best method for utilizing the data from the crystal monitor is to take the difference between the thickness values at the completion of the evaporation when the shutter is closed and when the shutter is opened at the beginning of the evaporation. This method produced reliable and repeatable results when the data from the crystal monitor was compared to the integrated ion flux. When the values of the crystal monitor measured thickness (in $\text{k}\text{\AA}$) are plotted vs. the integrated ion flux (in μC) the values are very linear. In fact, when a linear fit was applied to these values, the fit consistently had a slope of $0.001 \text{ k}\text{\AA}/\mu\text{C}$. There is one possible source of error when using this method. If the emission drops enough to significantly lower the evaporation rates, the effect of thermal drift may outweigh the effect of the material being deposited on the crystal monitor, yielding negative thickness values. This occurred twice during permalloy film growth, which required lower levels of emission than iron.

Another method of utilizing the crystal monitor data is to record its thickness value well after the evaporation (a minimum of 30 minutes) when the head has had a chance to cool off and return to thermal equilibrium. When these values of thickness were plotted vs. the integrated ion flux the data were also linear. However, the quality of the fit was in general poorer than when using the difference method and the value of the slope obtained was not repeatable from one data run to another. A sample plot of the crystal monitor

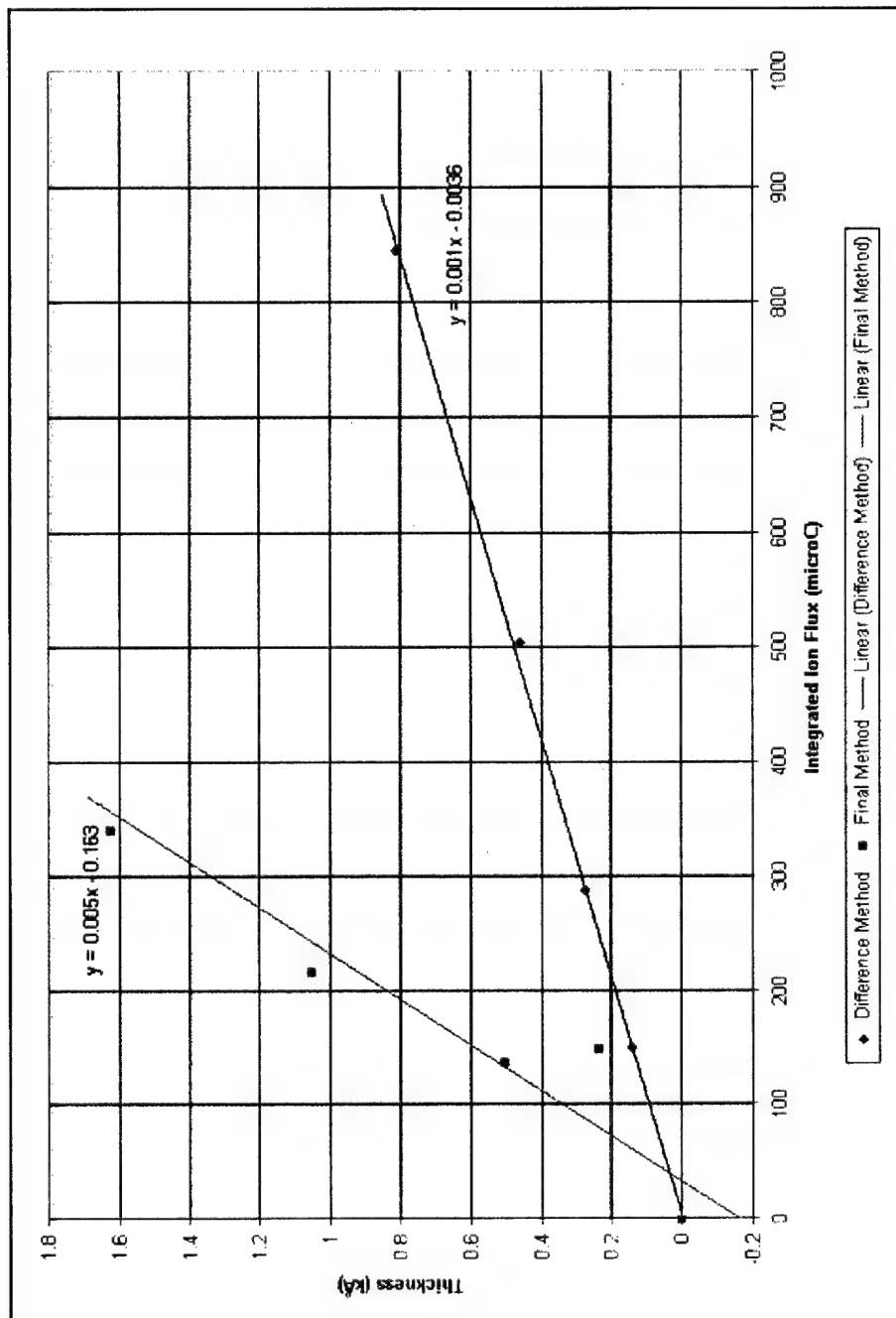


Figure 25: Crystal Monitor Thickness vs. Integrated Ion Flux. The data were taken during a series of Fe evaporations. Both methods of using the crystal monitor data are displayed here.

thickness readings vs. the integrated ion flux from a Fe film growth run is shown in Figure 25. Both methods of using the crystal monitor data are shown in this plot for comparison.

Two possible sources of error when using the final steady-state readings of the crystal monitor are that material could be deposited during the soak period and most certainly some metal is deposited between the time that the filament current is raised to evaporation conditions and when the MBE cell shutter is opened. In the future, additional data runs in which the final thickness values of the crystal monitor are compared to the ion current integrated from the beginning of the soak period through the completion of the evaporation should be conducted.

The AES data taken after each evaporation could be interpreted using published AES studies. A comprehensive study of Fe/W[100] growth modes conducted by White et. al. proved to be very helpful. A graph of the Fe(703)/W(179) Auger signal ratio vs. deposition time from this study is displayed in Figure 26. According to the graph, 1 ML of Fe has been deposited when AES produces a Fe(703)/W(179) signal ratio of 0.95 and 2 ML of Fe have been deposited when a ratio of 4 is recorded.¹⁸

The Auger signal ratios that we measured for each evaporation were recorded and plotted vs. the integrated ion flux. Plots were made for both iron and permalloy evaporations and are shown in Figures 27 and 28. These results show that approximately 860 μC of integrated ion current corresponded to 1 ML of iron deposited on the W substrate in the CMA system. As an approximation, the ratio for Fe(703)/W(179) was compared to the values of Ni(849)/W(179).

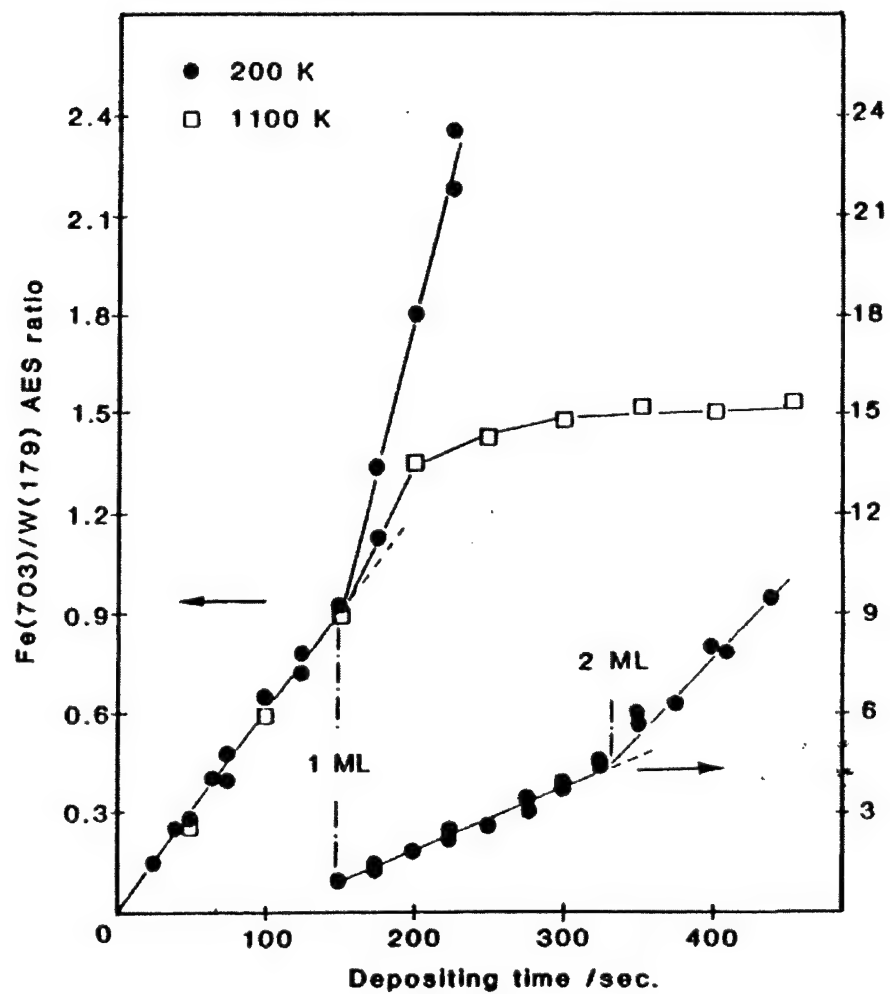


Figure 26: Fe(703)/W(179) Auger signal ratio vs. deposition time. The temperature refers to the substrate temperature during the evaporation.¹⁷

This showed that approximately 40 μC of integrated ion current corresponded to a ML of permalloy deposited on the substrate. Further evaporations must be conducted in order to refine the numbers given here.

Some peculiar results can be seen in the plot of the Fe/W ratios vs. integrated ion flux in Figure 27. After starting with a “clean” W substrate with no Fe peaks, the AES spectra taken after the first one minute evaporation yielded a Fe(703)/W(179) ratio of 0.396. Two more one minute evaporations were then conducted, after which the Fe(703)/W(179) ratio decreased. Finally, a two minute evaporation raised the ratio to 1.053. We currently do not understand why the ratio decreased after the second and third evaporations. Although much care was taken to carefully ground the sample while taking AES spectra, an adequate ground may not have been established. Perhaps there is an additional phenomena or source of error that we do not yet understand. However, early indications show that evaporations of at least two minutes in length may produce better results than those of shorter durations.

As a final note to the experimental results, measuring the ion current has shown much promise as a method of characterizing film growth. The ion current never experienced a thermal drift and proved to be extremely sensitive. An almost instantaneous response could be seen in the ion current when adjustments were made to the emission. For example, when stopping an evaporation and turning off the filament current, an immediate drop to zero in the ion current can be seen in the data collected by the Labview software.

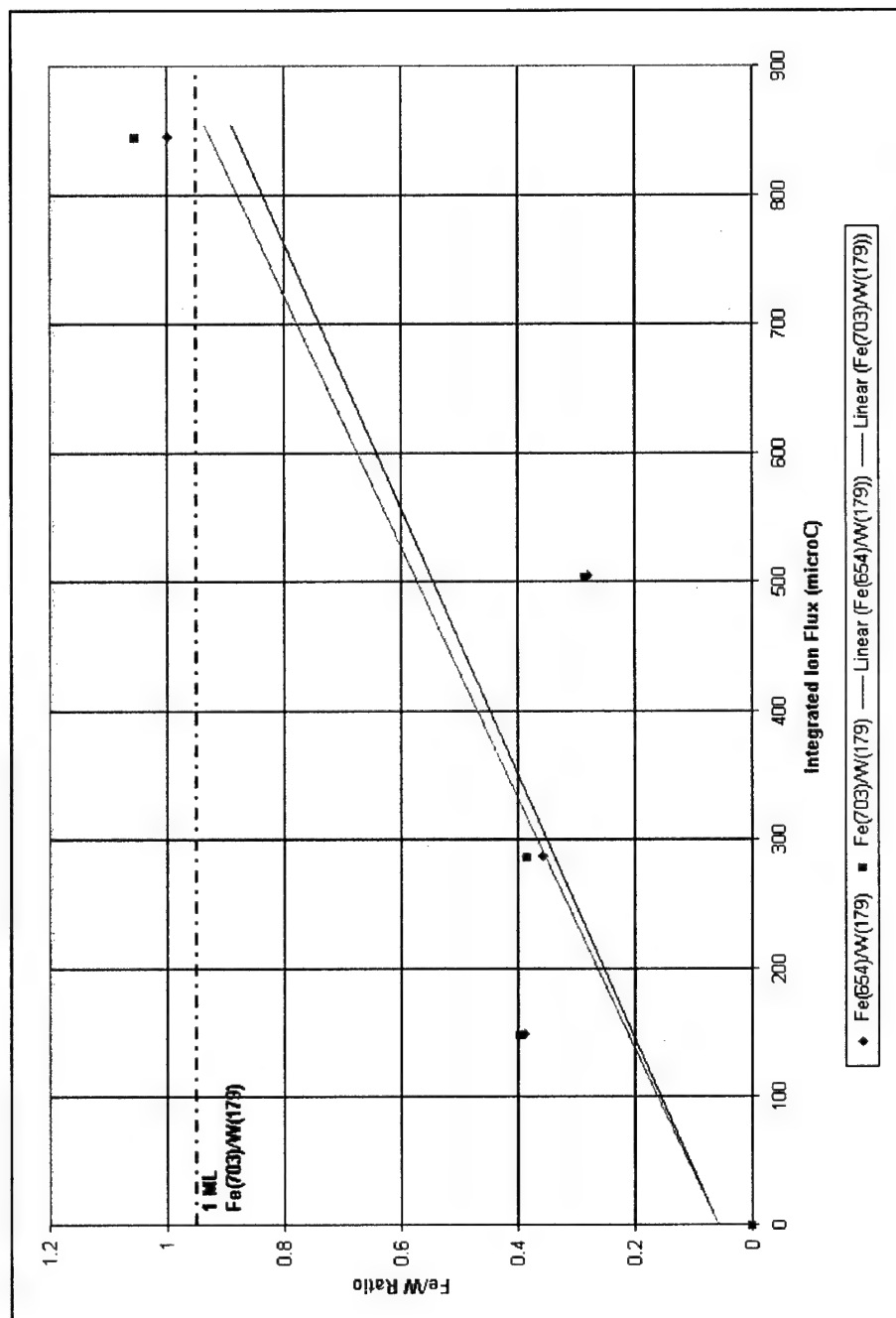


Figure 27: Plot of Fe/W Auger Signal Ratios vs. Integrated Ion Flux Obtained During an Fe Evaporation.

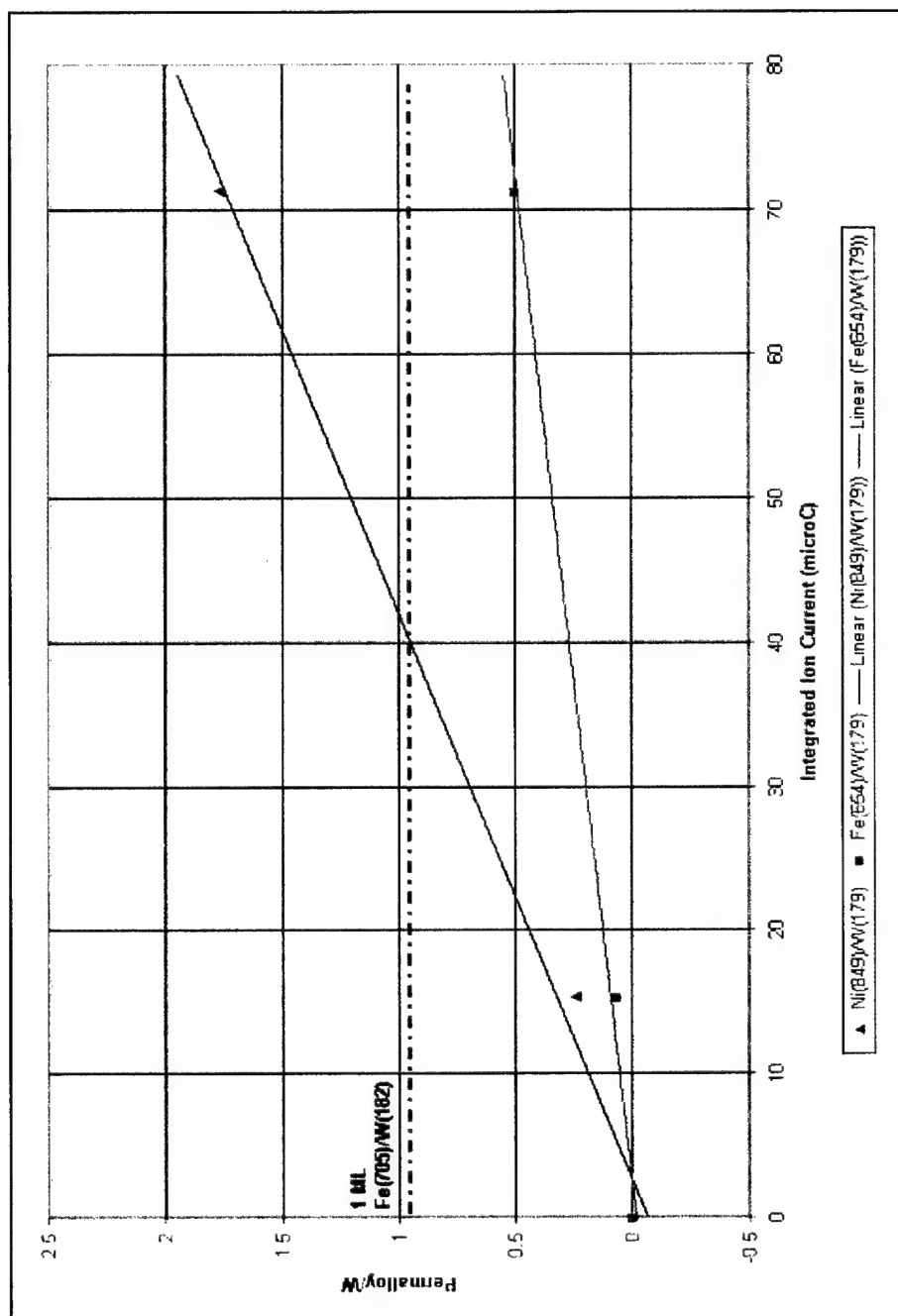


Figure 28: Plot of Permalloy/W Auger Signal Ratios vs. Integrated Ion Flux Obtained During a Permalloy Evaporation.

Chapter 8: Conclusion

This project succeeded in improving our CMA thin film growth and analysis chamber. An MBE cell was upgraded and proved to be a useful pendant-drop type EB evaporator. The upgrades of the evaporator and substrate power supplies will provide a much more robust system for thin film growth and high temperature flashing of the sample. Also, the bake-out electronics were upgraded and important features were added, such as the ion pump mode to protect the system in the event of a leak during bake-out and the addition of a circuit to power a fan once bake-out is complete.

The integration of NI's Labview software and a DAQ board with instrumentation to both monitor thin film growth and plot Auger spectra proved to be a very useful tool for metallic thin film growth. There were several challenges to overcome but in the end two very robust software packages were produced. These Labview VI's will continue to be very useful on the CMA system and can be implemented on other systems throughout our lab.

Evaporation conditions for both iron and permalloy were explored and the conditions and instrument settings that were found to work best are documented here. Calibrations were developed for the growth rates of iron and permalloy against both integrated ion current and measured crystal monitor thickness. The crystal monitor was found to exhibit a considerable temperature drift. However, useful calibration data can be obtained by taking the difference in the monitor's thickness values between the end and beginning of an evaporation. Further experiments using the monitor's final steady-state readings need to be conducted

to determine if this strategy can produce accurate flux calibrations. In the future, additional heat shielding could be added to the crystal monitor. Also, a second monitor could be added in a location where it is less susceptible to heating from the filament yet close enough to the source to record thickness values from the flux that it intercepts.

From the results of this project, it is believed that monitoring the integrated ion current will prove to be a very reliable method of monitoring film growth. The calibrations presented here are an excellent start to further refinement of the calibration and beginning growth of research grade magnetic films.

Replacing the metal wire source with an e-beam heated Mo Knudsen cell could make the MBE cell much more robust. Higher currents would be needed to heat the source metal to evaporation temperatures but many other potential problems would be eliminated. There would no longer be the danger of the metal source wire distorting and either shorting to the filament or lowering the evaporation rate if heated too aggressively. Plus, a Mo crucible could hold much more source material and would not be depleted as quickly. Finally, the geometry of the evaporator would not significantly change as the source is evaporated.

Unfortunately, instrumentation problems and other difficulties prevented more calibration runs being taken. However, the preliminary data were promising and will prove very useful to future researchers. The CMA thin film growth system is in an excellent state for future calibrations to be conducted and for thin films and microstructures to be grown for further analysis.

References

1. P. Grünberg, *Physics Today*, May, 31 (2001).
2. M. J. Zhu, D. M. Bylander, and L. Kleinman, *Physical Review*, B 43, 4007 (1991).
3. J. Chen and J. L. Erskine, *Physical Review Letters*, 68, 1212 (1992).
4. H. C. Mireles, *Step Induced Magnetic Anisotropy of Fe/W(100)*, Doctoral Dissertation, University of Texas at Austin, 2000.
5. A. Hubert and R. Schäfer, *Magnetic Domains The Analysis of Magnetic Microstructures*, Springer, 1998.
6. J. Araya-Pochet, G. A. Mulhollan, and J. L. Erskine, *Review of Scientific Instruments*, 62, 2288 (1991).
7. XTC Thin Film Thickness and Rate Monitor, Inficon, East Syracuse, New York.
8. T. Jones, J. Sawler, and D. Venus, *Review of Scientific Instruments*, 64, 2008 (1993).
9. A. Zangwill, *Physics at Surfaces*, Cambridge University Press, 1988.
10. Auger Electron Spectrometry Instrumentation Tutorial. [Online]. Charles Evans and Associates. <<http://www.eaglabs.com/cai/auginst/caiainst.htm>>
11. C. L. Hedberg ed., *Handbook of Auger Electron Spectroscopy*, Physical Electronics, Inc., 1995.
12. Auger Electron Spectrometry Theory Tutorial. [Online]. Charles Evans and Associates. <<http://www.eaglabs.com/cai/augtheo/caiatheo.htm>>
13. National Instruments, 11500 N Mopac Expwy, Austin, TX 78759-3504.
14. Keithley Instruments, Inc., 28775 Aurora Road, Cleveland, Ohio 44139.
15. Manufacturer's Specifications: Keithley Instruments, Inc.
16. Manufacturer's Specifications: Inficon.

17. Minolta/Land Cyclops 52, Land Instruments, 10 Friends Lane, Newtown, PA 18940-1804.
18. X. L. Zhou, C. Yoon, and J. White, Surface Science 203, 53 (1988).

Vita

Todd Charles Monson was born in Philadelphia, Pennsylvania on August 16, 1975. He is the only child of Randall and Susan Monson. After graduating from Rutherford High School in Panama City, Florida in May of 1993 he entered the United States Naval Academy during July of that same year. He was a distinguished graduate from the Naval Academy in May 1997 (B.S. – Physics). Upon his graduation, he was commissioned as a 2nd Lieutenant in the United States Air Force and assigned to the Air Force Research Laboratory, Munitions Directorate at Eglin AFB, Florida. There, he spent the next three years as a research scientist in the lab's Advanced Guidance Division. In the Spring of 2000 he was selected by the Air Force to attend Graduated School in order to prepare for an instructor position in the United States Air Force Academy Department of Physics. In September of 2000, he entered the Graduate School of the University of Texas and is registered to graduate in December 2001, with a M.A. in Physics.

Permanent address: 3608 A Bannockburn Dr., Austin, Texas 78749

This thesis was typed by the author.

System for Fabricating Thin Film Magnetic Microstructures

Abstract

An Ultra High Vacuum (UHV) system was reconditioned and improved in order to use it to develop high quality and well characterized magnetic films. This involved upgrading and repairing instrumentation used in both thin film growth and characterization. Most importantly, a sensitive flux sensor to monitor film growth was developed and calibrated. Descriptions of the upgrades, calibration process, and the calibration data are presented here.

References

1. P. Grünberg, *Physics Today*, May, 31 (2001).
2. M. J. Zhu, D. M. Bylander, and L. Kleinman, *Physical Review*, B 43, 4007 (1991).
3. J. Chen and J. L. Erskine, *Physical Review Letters*, 68, 1212 (1992).
4. H. C. Mireles, *Step Induced Magnetic Anisotropy of Fe/W(100)*, Doctoral Dissertation, University of Texas at Austin, 2000.
5. A. Hubert and R. Schäfer, *Magnetic Domains The Analysis of Magnetic Microstructures*, Springer, 1998.
6. J. Araya-Pochet, G. A. Mulhollan, and J. L. Erskine, *Review of Scientific Instruments*, 62, 2288 (1991).
7. XTC Thin Film Thickness and Rate Monitor, Inficon, East Syracuse, New York.
8. T. Jones, J. Sawler, and D. Venus, *Review of Scientific Instruments*, 64, 2008 (1993).
9. A. Zangwill, *Physics at Surfaces*, Cambridge University Press, 1988.
10. Auger Electron Spectrometry Instrumentation Tutorial. [Online]. Charles Evans and Associates. <<http://www.eaglabs.com/cai/auginst/caiainst.htm>>
11. C. L. Hedberg ed., *Handbook of Auger Electron Spectroscopy*, Physical Electronics, Inc., 1995.

12. Auger Electron Spectrometry Theory Tutorial. [Online]. Charles Evans and Associates. <<http://www.eaglabs.com/cai/augtheo/caiatheo.htm>>
13. National Instruments, 11500 N Mopac Expwy, Austin, TX 78759-3504.
14. Keithley Instruments, Inc., 28775 Aurora Road, Cleveland, Ohio 44139.
15. Manufacturer's Specifications: Keithley Instruments, Inc.
16. Manufacturer's Specifications: Inficon.
17. Minolta/Land Cyclops 52, Land Instruments, 10 Friends Lane, Newtown, PA 18940-1804.
18. X. L. Zhou, C. Yoon, and J. White, Surface Science 203, 53 (1988).

Personal Information:

Todd Charles Monson, Capt, USAF
Degree: M.A. Physics
Institution: University of Texas at Austin
Year Awarded: 2001
Number of Pages: 78

System for Fabricating Thin Film Magnetic Microstructures

Abstract

An Ultra High Vacuum (UHV) system was reconditioned and improved in order to use it to develop high quality and well characterized magnetic films. This involved upgrading and repairing instrumentation used in both thin film growth and characterization. Most importantly, a sensitive flux sensor to monitor film growth was developed and calibrated. Descriptions of the upgrades, calibration process, and the calibration data are presented here.

References

1. P. Grünberg, *Physics Today*, May, 31 (2001).
2. M. J. Zhu, D. M. Bylander, and L. Kleinman, *Physical Review*, B 43, 4007 (1991).
3. J. Chen and J. L. Erskine, *Physical Review Letters*, 68, 1212 (1992).
4. H. C. Mireles, *Step Induced Magnetic Anisotropy of Fe/W(100)*, Doctoral Dissertation, University of Texas at Austin, 2000.
5. A. Hubert and R. Schäfer, *Magnetic Domains The Analysis of Magnetic Microstructures*, Springer, 1998.
6. J. Araya-Pochet, G. A. Mulhollan, and J. L. Erskine, *Review of Scientific Instruments*, 62, 2288 (1991).
7. XTC Thin Film Thickness and Rate Monitor, Inficon, East Syracuse, New York.
8. T. Jones, J. Sawler, and D. Venus, *Review of Scientific Instruments*, 64, 2008 (1993).
9. A. Zangwill, *Physics at Surfaces*, Cambridge University Press, 1988.
10. Auger Electron Spectrometry Instrumentation Tutorial. [Online]. Charles Evans and Associates. <<http://www.eaglabs.com/cai/auginst/caiinst.htm>>
11. C. L. Hedberg ed., *Handbook of Auger Electron Spectroscopy*, Physical Electronics, Inc., 1995.

12. Auger Electron Spectrometry Theory Tutorial. [Online]. Charles Evans and Associates. <<http://www.eaglabs.com/cai/augtheo/caiatheo.htm>>
13. National Instruments, 11500 N Mopac Expwy, Austin, TX 78759-3504.
14. Keithley Instruments, Inc., 28775 Aurora Road, Cleveland, Ohio 44139.
15. Manufacturer's Specifications: Keithley Instruments, Inc.
16. Manufacturer's Specifications: Inficon.
17. Minolta/Land Cyclops 52, Land Instruments, 10 Friends Lane, Newtown, PA 18940-1804.
18. X. L. Zhou, C. Yoon, and J. White, Surface Science 203, 53 (1988).

Personal Information:

Todd Charles Monson, Capt, USAF
Degree: M.A. Physics
Institution: University of Texas at Austin
Year Awarded: 2001
Number of Pages: 78